COHERENT EDDIES AND TURBULENCE IN VEGETATION CANOPIES: THE MIXING-LAYER ANALOGY

M. R. RAUPACH, J. J. FINNIGAN and Y. BRUNET
CSIRO Centre for Environmental Mechanics, GPO Box 821, Canberra, ACT 2601, Australia

(Received in final form 6 February, 1996)

Abstract. This paper argues that the active turbulence and coherent motions near the top of a vegetation canopy are patterned on a plane mixing layer, because of instabilities associated with the characteristic strong inflection in the mean velocity profile. Mixing-layer turbulence, formed around the inflectional mean velocity profile which develops between two coflowing streams of different velocities, differs in several ways from turbulence in a surface layer. Through these differences, the mixing-layer analogy provides an explanation for many of the observed distinctive features of canopy turbulence. These include: (a) ratios between components of the Reynolds stress tensor; (b) the ratio K_H/K_M of the eddy diffusivities for heat and momentum; (c) the relative roles of ejections and sweeps; (d) the behaviour of the turbulent energy balance, particularly the major role of turbulent transport; and (e) the behaviour of the turbulent length scales of the active coherent motions (the dominant eddies responsible for vertical transfer near the top of the canopy). It is predicted that these length scales are controlled by the shear length scale $L_s = U(h)/U'(h)$ (where h is canopy height, $U(z)$ is mean velocity as a function of height z, and $U' = \mathrm{d}U/\mathrm{d}z$). In particular, the streamwise spacing of the dominant canopy eddies is $\Lambda_x = mL_s$, with $m = 8.1$. These predictions are tested against many sets of field and wind-tunnel data. We propose a picture of canopy turbulence in which eddies associated with inflectional instabilities are modulated by larger-scale, inactive turbulence, which is quasi-horizontal on the scale of the canopy.

1. Introduction

Vegetation-atmosphere transfer of momentum and scalar entities (heat, water vapour, CO_2 and so on) influences numerous environmental variables and processes. Familiar examples include canopy microclimates; the energy and water balances of vegetated surfaces; vegetation and soil surface temperatures; the deposition and re-entrainment of dust and other particles; and wind damage to forests and crops. Spurred by such applications, knowledge of canopy turbulence has advanced steadily over the last three decades. Perhaps the main development over this time has been the recognition (as in turbulence research in general) that canopy turbulence is far from random, with major contributions to the turbulent motions arising from coherent eddies of canopy scale. This can lead to phenomena such as locally counter-gradient fluxes, thereby precluding the use of simple gradient-diffusion theory (K-theory) to describe vertical turbulent transfer in canopies. Furthermore, the coherent eddy structure within and just above the canopy is somewhat different from the eddy structure in the surface layer well above the canopy. This is shown by a number of simple indicators: for example, ratios among components of the Reynolds stress tensor; velocity skewnesses; the behaviour of the turbulent energy balance; and the behaviour of turbulence length scales. The experimental

Boundary-Layer Meteorology **78:** 351–382, 1996.

justifications for these statements arise from many sources which have been previously reviewed in detail (Raupach and Thom, 1981; Finnigan and Raupach, 1987; Raupach, 1988; Raupach *et al.*, 1991; Kaimal and Finnigan, 1994).

In an effort to unify many of these experimental findings, this paper argues that the active turbulence near the top of the canopy (the eddies primarily responsible for vertical transfer) resembles the flow in a *plane mixing layer* rather than a boundary layer. The plane mixing layer is the turbulent shear flow formed in the region between two coflowing streams of different velocities. It is characterised by a strong inflection in the mean velocity profile, in contrast with boundary-layer flow. A key property of a velocity inflection is that it induces characteristic hydrodynamic instability processes which set the pattern for the coherent eddies in the resulting fully-developed turbulent flow, and determine the turbulence length scales.

Our suggested analogy between mixing-layer and canopy turbulence flies in the face of a long-held view that canopy turbulence is a perturbed version of the turbulence in the overlying boundary layer. This is a natural view because a canopy is immersed in the lowest part of a deep turbulent boundary layer. However, it ignores the basic nature of the canopy velocity profile: typically, the mean velocity profile has a strong inflection point near the top of the canopy, which becomes even stronger during gust events (Finnigan, 1979a,b). We argue that the instability processes arising from this inflection are essentially similar to those in a mixing layer, and determine much of the coherent eddy structure near the top of a vegetation canopy.

In this paper we restrict attention to near-neutral flow over a horizontally extensive, uniform vegetation canopy, and do not consider buoyancy effects. The assumption of horizontal uniformity excludes "sparse" canopies, in which the plant spacing is of the order of the canopy height or larger. The neglect of buoyancy may not be as drastic a simplification as it appears at first sight. Within and just above low canopies such as crops, buoyancy effects during daytime are often insignificant, even when conditions well above the canopy are strongly unstable. The reason is that the ratio of shear to buoyant production of turbulent energy varies inversely with height above the aerodynamic ground level or zero-plane displacement (Wyngaard, 1988). In tall forest canopies, conditions during the day are often strongly stable in the lower canopy because the solar heating is concentrated in the crown, while during the night the lower canopy is typically unstable and the upper canopy stable, as documented for Amazon rainforest by Fitzjarrald *et al.* (1990) and Fitzjarrald and Moore (1990). This has a significant *quantitative* influence on turbulence statistics (Shaw *et al.*, 1988). However, Brown and Roshko (1974) showed that even the extreme buoyancy difference between helium and nitrogen has little *qualitative* effect on the nature of the coherent eddies in a mixing layer. One consequence of the mixing-layer analogy, therefore, is that the turbulent eddy structure near the top of the canopy has a similar qualitative behaviour (though not identical quantitative properties) across a wide range of buoyancy conditions.

The paper has six sections. Following this introduction, the next two sections review the experimental information required for later developments, by summarising the basic properties of canopy turbulence (Section 2) and the experimental evidence for the existence and form of coherent eddies in canopy flow (Section 3). Section 4 describes the flow and instability processes in a mixing layer. Section 5 then tests inferences from the mixing-layer analogy about the behaviour of many turbulence properties in canopies. Finally, Section 6 presents a physical picture for the dominant eddy structure in a canopy, and indicates some further applications for the mixing-length analogy.

The paper is a major extension of ideas first advanced briefly in Raupach *et al.* (1989). New work includes the treatment of linear stability theories, a more conclusive treatment of length scale data, the use of wavelet transform data, and discussion of eddy diffusivity ratios.

2. Basic Properties of Canopy Turbulence

2.1. Velocity moments

Figure 1 is a "family portrait" of canopy turbulence, redrawn and substantially updated from Raupach (1988). It shows profiles of single-point turbulence statistics measured in 12 separate experiments on near-neutral flow through horizontally uniform, extensive canopies, including crops, forests and model canopies in wind tunnels. Details for each experiment are given in Table I. The data span a very large range of canopy height (h) and roughness density (λ, defined as the total frontal area of roughness elements, projected in the wind direction, per unit ground area; if the canopy elements are isotropically oriented flat leaves and stem area is neglected, then λ is half the single-sided leaf area index). The statistics in Figure 1 are the mean velocity $U(z)$, the Reynolds shear stress $\overline{uw}$, the velocity standard deviations $\sigma_u(z) = (\overline{u^2})^{1/2}$ and $\sigma_w(z) = (\overline{w^2})^{1/2}$, the uw correlation coefficient $r_{uw} = \overline{uw}/(\sigma_u \sigma_w)$, the u and w skewnesses Sk_u and Sk_w, and the length scales L_u and L_w (discussed later). Here, u, v and w are the instantaneous fluctuating velocity components in the streamwise (x), lateral (y) and vertical (z) directions, respectively. The (x, y, z) coordinate frame is oriented with the mean wind direction, so that the mean velocity vector is $(U(z), 0, 0)$. Overbars denote time averages. Heights (z) are measured from the ground as origin and are normalised with the canopy height h. Normalising velocity scales are the mean velocity U_h at the canopy top and the friction velocity u_*, defined so that $u_* = (-\overline{uw})^{1/2}$ in the constant-stress region above the canopy.

The observations in Figure 1 have many common features, but also exhibit variations due to differences in canopy morphology. Profiles of leaf area density $\alpha(z)$ (Figure 1j) show that the main morphological difference between the canopies is the extent to which the canopy elements are clustered in a crown near the top

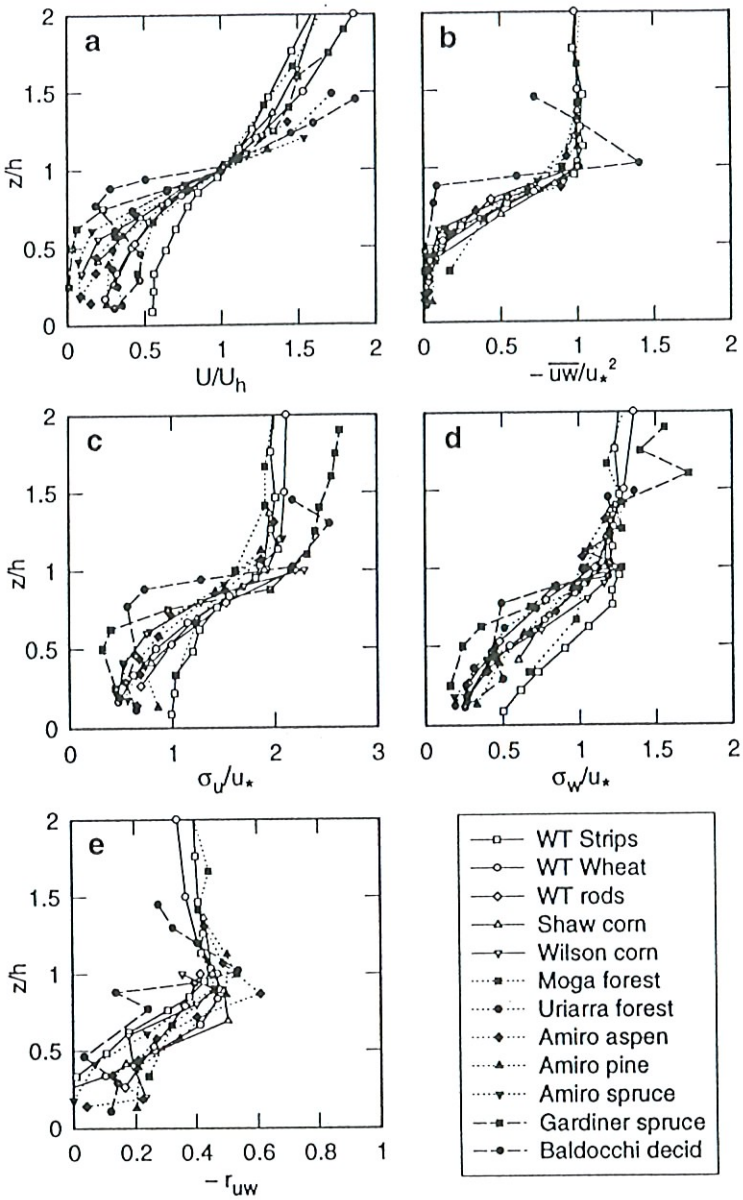

Figure 1a–e. A "family portrait" of canopy turbulence for canopies A to L in Table I, showing profiles with normalized height z/h of (a) U/U_h; (b) $-\overline{uw}/u_*^2$; (c) σ_u/u_*; (d) σ_w/u_*; (e) $-r_{uw} = -\overline{uw}/(\sigma_u\sigma_w)$; (f) Sk_u; (g) Sk_w; (h) L_u; (i) L_w; and (j) $h\alpha(z)$, where $\alpha(z)$ is the leaf area density. Length scales L_u and L_w are defined by Equation (1).

of the canopy (canopies J, K and L). As we show later, the mixing-length analogy provides a means of reconciling these differences.

More important than the differences are the common features. First, and most obvious, is vertical inhomogeneity: U, $\overline{uw}$, σ_u and σ_w decay rapidly with decreasing height within the canopy (Figure 1a,b,c,d).

Second, there is a strong inflection in $U(z)$ near the canopy top, where the shear $U' = \mathrm{d}U/\mathrm{d}z$ is maximal (Figure 1a). The strength of the shear at this point is described by the length scale $U(h)/U'(h) = L_s$, which decreases as shear increases. Table I shows that L_s is typically around $0.5h$ but depends significantly

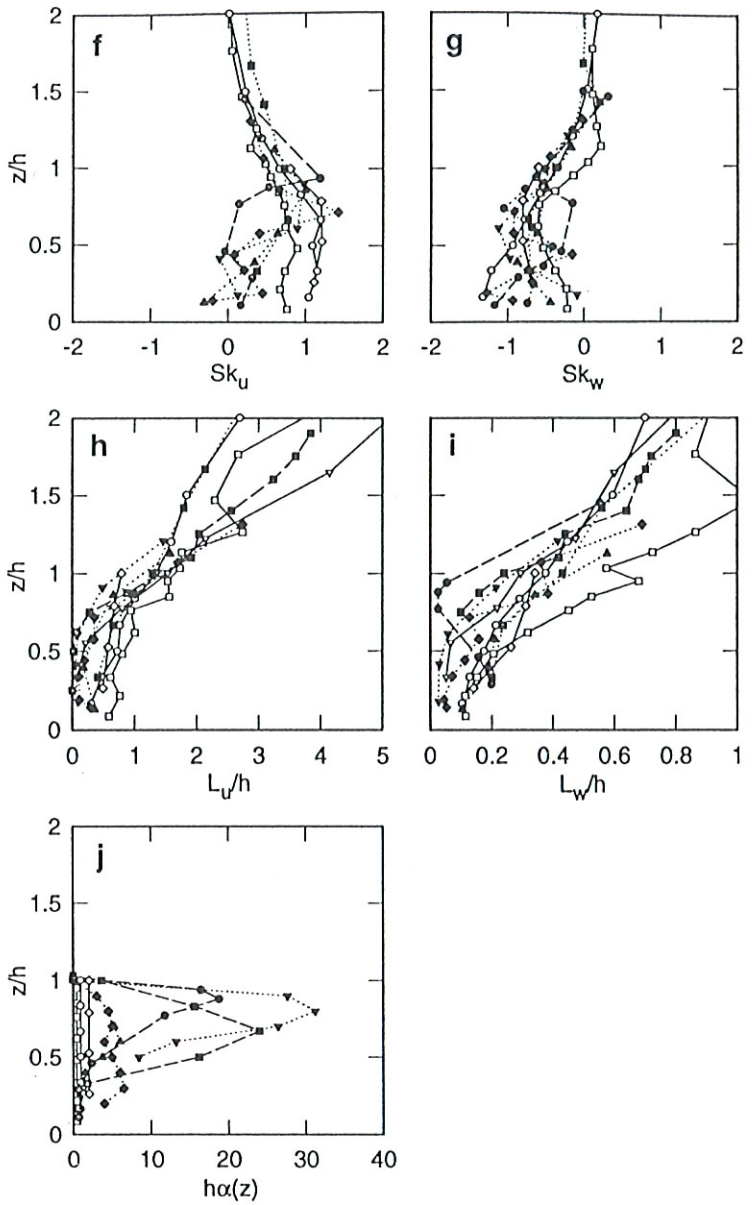

Figure 1f–j.

on λ (decreasing as λ increases) and on the leaf area density profile (decreasing as leaf area is concentrated near the top of the canopy).

Third, well above the canopy ($z > 2h$), the flow assumes the "inertial sublayer" properties of the conventional atmospheric surface layer. In thermally near-neutral conditions, the mean velocity profile is logarithmic with aerodynamic height $z - d$, where d is the zero-plane displacement. The ratios σ_u/u_* and σ_w/u_* (expressions of ratios among Reynolds stress tensor components in a constant-stress layer) are typically about 2.5 and 1.25 (Garratt, 1992), implying that $r_{uw} = \overline{uw}/(\sigma_u \sigma_w)$ is about -0.32. These values are approached at heights greater than those shown in Figure 1.

Fourth, values of σ_u/u_*, σ_w/u_* and r_{uw} just above the canopy are rather different: here σ_u/u_* falls from 1.5 to 2, σ_w/u_* to around 1.1 and r_{uw} increases to about

Table I

Physical and aerodynamic properties of canopies in Figure 1. WT = wind tunnel. The roughness density or frontal area index, λ, is assumed to be half the single-sided leaf area index for field canopies

Canopy	Ident	h (m)	λ	U_h/u_*	L_s/h	Reference
WT strips	A	0.06	0.23	3.3	0.85	Raupach *et al.* (1986)
WE wheat	B	0.047	0.47	3.6	0.57	Brunet *et al.* (1994)
WT rods	C	0.19	1	5.0	0.49	Seginer *et al.* (1976)
Shaw corn	D	2.6	1.5	3.6	0.39	Shaw *et al.* (1974)
Wilson corn	E	2.25	1.45	3.2	0.46	Wilson *et al.* (1982)
Moga eucalypt	F	12	0.5	2.9	0.58	Unpublished
Uriarra pine	G	20	2.05	2.5	0.29	Denmead and Bradley (1987)
Amiro aspen	H	10	1.95	2.6	0.58	Amiro (1990a)
Amiro pine	I	15	1	2.2	0.50	Amiro (1990a)
Amiro spruce	J	12	5	2.4	0.44	Amiro (1990a)
Gardiner spruce	K	12	5.1	4.0	0.30	Gardiner (1994)
Baldocchi deciduous	L	24	2.5	2.8	0.12	Baldocchi and Meyers (1988a,b)

-0.5, relative to inertial sublayer values. The larger magnitude of r_{uw} suggests that the turbulence near the top of the canopy is in some sense more organised, or more efficient at momentum transfer, than inertial-sublayer turbulence. This is one of many properties of the *roughness sublayer*, a layer extending upward from $z = h$ to (typically) about $2h$, in which the turbulence is modified from its inertial-sublayer form by the proximity of the canopy.

Fifth, the u and w skewnesses Sk_u and Sk_w are small well above the canopy, but large within the canopy where Sk_u is typically 0.5 to 1 and Sk_w typically -0.5 to -1 (Figure 1f,g). The association of positive u and negative w skewness suggests that the strongest turbulent events within the canopy are gust or sweep motions, consisting of brief but intense incursions of downward-moving, high-speed air ($w < 0, u > 0$) into the canopy, as confirmed by quadrant analysis (see later).

2.2. Length Scales and Spectra

The usual method for obtaining information on length scales and spectra in the atmospheric surface layer is to apply the Taylor frozen-turbulence hypothesis to single-point turbulence measurements. Unfortunately this approach is fraught with difficulty within canopies because of high turbulence intensities (typically $\sigma_u/U \gtrsim 1$). Nevertheless, by far the largest base of experimental information comes from single-point measurements. Some of these are shown in Figure 1h and 1i, in the form of profiles of the single-point length scales

$$L_u = \frac{U}{\sigma_u^2}\int_0^\infty \overline{u(s)u(s+t)}\,\mathrm{d}t, \qquad L_w = \frac{U}{\sigma_w^2}\int_0^\infty \overline{w(s)w(s+t)}\,\mathrm{d}t. \tag{1}$$

Typically, L_u is around h and L_w around $h/3$ in the upper part of the canopy, indicating that the dominant eddies in the upper canopy are of order h in length scale. Later (Section 3.2) we discuss the problems with single-point length scale estimates by comparing them with two-point length scales; the length scales in Figures 1h and 1i turn out to be smaller than the two-point scales by factors of 2 or more within the canopy.

Single-point turbulence spectra have been measured in many canopies, for instance in corn by Shaw *et al.* (1974) and Wilson *et al.* (1982), and in forests by Baldocchi and Meyers (1988b), Bergström and Högström (1989) and Amiro (1990b). In general, the locations of the spectral peaks do not vary strongly with height in the upper canopy and just above the canopy. An appropriate measure is the peak frequency f_p on a plot of $fS(f)$ against $\ln(f)$, where f is frequency and S power spectral density. Measurements of f_p cluster around $f_{p(u)}h/U_h \approx 0.15 \pm 0.05$ for the u spectrum and $f_{p(w)}h/U_h \approx 0.45 \pm 0.05$ for the w spectrum (Kaimal and Finnigan, 1994). This behaviour is in strong contrast to the inertial sublayer well above the canopy, where f_p is observed to be proportional to $(z-d)/U$ in near-neutral conditions in accordance with surface-layer similarity theory and Taylor's hypothesis (Kaimal *et al.*, 1972).

2.3. TKE BUDGET

For canopy flow, the turbulent kinetic energy (TKE) budget is

$$\frac{\partial \overline{e^2}}{\partial t} = \underset{\substack{\text{shear}\\\text{production}}}{P_s} + \underset{\substack{\text{wake}\\\text{production}}}{P_w} + \underset{\substack{\text{buoyant}\\\text{production}}}{P_b} + \underset{\substack{\text{turbulent}\\\text{transport}}}{T_t} + \underset{\substack{\text{pressure}\\\text{transport}}}{T_p} - \underset{\text{dissipation}}{\varepsilon} \tag{2}$$

where $\overline{e^2} = (\overline{u^2}+\overline{v^2}+\overline{w^2})/2$ is the TKE (including all scales). This must be derived using both temporal and spatial averaging operations, to account for dynamical processes induced by heterogeneity at small (element) scales (Wilson and Shaw, 1977). The forms of the terms are given by Brunet *et al.* (1994), for example. The shear production (P_s), buoyant production (P_b), turbulent transport (T_t), pressure transport (T_p) and dissipation (ε) terms have conventional forms (e.g. Kaimal and Finnigan, 1994). The wake production term P_w accounts for the generation of element-scale TKE in the wakes of canopy elements.

TKE budgets have now been measured in several canopies, including Moga Forest, WT strips and WT wheat (Table I), and by Leclerc *et al.* (1990) and Meyers and Baldocchi (1991). Figure 2, from the WT wheat canopy, illustrates several generic aspects of the canopy TKE budget in near-neutral conditions. First, above the roughness sublayer ($z \gtrsim 2h$), the budget reduces to $P_s = \varepsilon$, a "local equilibrium" between shear production and dissipation (Townsend, 1976). Second, in the roughness sublayer ($h < z \lesssim 2h$) and within the canopy ($z < h$), turbulent transport becomes increasingly important: it is a loss term near $z = h$, and a gain (often the largest positive term) lower down. This implies that most of the

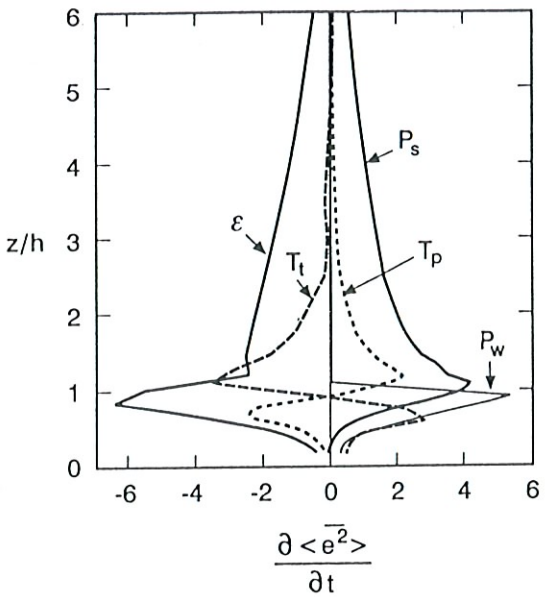

Figure 2. TKE balance in the WT wheat canopy (Table I). After Brunet *et al.* (1994). Terms as in Equation (2).

turbulence deep within the canopy is not locally generated, and that the entire canopy flow (including the roughness sublayer) is far from the local-equilibrium condition $P_s = \varepsilon$. Third, the pressure transport term T_p is difficult to measure and information about its behaviour is contradictory. Maitani and Seo (1985) used surface measurements of the kinematic pressure fluctuation p to estimate the pressure-induced TKE flux $\langle \overline{wp} \rangle$, finding this to be about half the turbulent TKE flux $\langle \overline{we^2} \rangle$; this suggests that $|T_p + T_t| > |T_t|$. Contrasting results were obtained by Brunet *et al.* (1994), who calculated T_p in the WT wheat canopy (Table I) by difference from other measured terms and also from closure assumptions; both suggested that T_p opposed T_t, so that $|T_p + T_t| \ll |T_t|$ (see Figure 2). Fourth, the wake production terrn P_w (estimated as $-\langle U \rangle \partial \langle \overline{uw} \rangle / \partial z$) is a large term in the canopy, substantially exceeding P_s. However, the resulting fine-scale "wake turbulence" is quickly dissipated, causing complementary large values of ε without contributing significantly to the overall TKE in the canopy (Brunet *et al.*, 1994).

2.4. Eddy diffusivities

The eddy diffusivities for momentum and heat are $K_M = -\overline{uw}/(\partial U/\partial z)$ and $K_H = -\overline{w\theta}/(\partial \Theta/\partial z)$ (where Θ and θ respectively denote mean and fluctuating potential temperatures). These are treated here as measured properties of the flow rather than predictive parameters in a theory. Measurements show that K_M and K_H behave differently in each of three regions. First, in the inertial sublayer, K_M and K_H are equal to the values K_M^* and K_H^* predicted by Monin–Obukhov similarity theory ($K_M^* = K_H^* = \kappa u_* (z - d)$ in neutral conditions, with $\kappa \approx 0.4$ the von Karman constant). Next, in the roughness sublayer just above the canopy

($h < z \lesssim 2h$), K_M and K_H increase above K_M^* and K_H^* as the surface is approached. With some inter-canopy variation, K_M is enhanced over K_M^* (just above $z = h$ and in near-neutral conditions) by a factor of 1.1 to 1.5, whereas K_H is enhanced over K_H^* by a factor of 2 to 3 (Garratt, 1978; Raupach, 1979; Raupach and Thom, 1981; Cellier, 1986; Chen and Schwerdtfeger, 1989; Shuttleworth, 1989; Cellier and Brunet, 1992). Thus, with decreasing height, the inverse turbulent Prandtl number ($\mathrm{Pr}_t^{-1} = K_H/K_M$) increases from around 1.1 in the near-neutral inertial sublayer (Garratt, 1992) to around 2 just above $z = h$. Finally, in the canopy layer below $z = h$, observations of K_M and K_H become very erratic, often exhibiting singularities and regions of negative values. This behaviour is associated with observations of countergradient fluxes within canopies (Denmead and Bradley, 1985; 1987), indicating that the turbulent transfer process is essentially nonlocal and cannot be described by a local gradient-diffusion relationship. Reasons for this behaviour can be advanced in both an Eulerian framework (Finnigan and Raupach, 1987) and a Lagrangian framework (Raupach, 1989), the latter offering a fairly straightforward replacement for a gradient-diffusion theory of turbulent transfer within canopies.

3. Observed Properties of Coherent Eddies in Canopies

Turning to coherent motions, some basic properties of canopy-scale coherent eddies can be inferred from single-point statistics. For instance, turbulence length scale measurements show that the eddies dominating turbulent transfer are of canopy scale (h), and are therefore "coherent" (well-correlated) on this scale. This section outlines three types of observations which yield further information about coherent eddies in canopies: studies of honami (wind waves); two-point turbulence statistics; and conditional analyses.

3.1. Honami

Honami waves, the coherent waving motions of patches of stalks in cereal crops on windy days, provide striking visual evidence that coherent eddies exist in canopy flows. These waves, first documented and named by Inoue (1955), have been studied in detail by Finnigan (1979a,b). The waves are produced as a gust microfront travels through the canopy, bending over the stalks as it passes. In the lee of the gust, the stalks oscillate at their natural frequency through several damped cycles, giving the impression of a wave moving through the canopy with a phase velocity equal to the gust velocity, typically about $2U_h$. The strongest honami activity occurs when the gust arrival frequency coincides with the natural frequency of the stalks. Finnigan (1979a,b) observed that the gusts have typical streamwise periodicities of order $5h$ to $8h$ and lateral widths of several h, and often arrive in packets of two or three.

3.2. TWO-POINT TURBULENCE STATISTICS

In contrast with single-point measurements, simultaneous measurements at multiple locations provide direct information on the spatial structure of turbulence. A fundamental statistic is the two-point space-time correlation function between velocities measured by a "reference" sensor located at $(0, 0, z_R)$ and a "roving" sensor at (x, y, z):

$$r_{ij}(x, y, z, \tau; z_R) = \frac{\overline{u_i(x, y, z, t+\tau) u_j(0, 0, z_R, t)}}{(\overline{u_i^2(z)})^{1/2} (\overline{u_j^2(z_R)})^{1/2}} \tag{3}$$

where $u_i = (u, v, w)$. This is a very useful quantity for assessing some aspects of turbulence structure, particularly length scales, but interpretations in terms of coherent motions must be made carefully because the correlation is diluted by chaotic, incoherent motions and may also be smeared by random phase shifts between coherent motions. Horizontal homogeneity and stationarity are assumed in Equation (3), but even so, r_{ij} is a function of five independent variables. Three special cases of r_{ij} (or its integral properties) are therefore commonly used.

(1) The *vertically separated space-time correlation*, $r_{ij}(0, 0, z, \tau; z_R)$, has been measured in various field and model canopies by Gao *et al.* (1989), Shaw *et al.* (1989) and Raupach *et al.* (1989); see Raupach *et al.* (1991) for review.

(2) The *spatial correlation at zero time delay*, $r_{ij}(x, y, z, 0; z_R)$, is mainly available from wind-tunnel measurements because of limitations on sensor deployment in the field. Shaw *et al.* (1995) analysed two-point velocity correlations from the WT wheat canopy (Table I). From this work, Figures 3 and 4 show slices (respectively in the xz and yz planes) of the zero-time-delay spatial correlation functions, $r_{ij}(x, y, z, 0; z_R)$, for u and w (that is, r_{11} and r_{33}). In the xz plane (Figure 3), r_{11} exhibits tilted, nearly elliptical, longitudinally stretched isocorrelation contours, with a tilt angle (defined from the major axes of the ellipses) of about 18° above the canopy and less within; in contrast, r_{33} exhibits almost circular contours and decays much more rapidly with spatial separation. In the yz plane (Figure 4), the isocorrelation lines are nearly circular, with a strong negative peak in r_{11} at a lateral displacement of about $3h$ from the reference probe, and a weaker negative peak in r_{33} at a slightly smaller lateral displacement. These suggest the presence of a streamwise vortical motion with a lateral periodicity of several canopy heights. Figures 3 and 4 together confirm that, in a time-averaged sense, fluid motions near the top of the canopy are well correlated over length scales of order h. At $z_R = h$, there is significant correlation for u ($r_{11} > 0.2$) within a sloping elliptical region defined roughly by $|x| < 4h$, $|y| < h$, and $|z - z_R| < 2h$; for w, the corresponding region ($r_{33} > 0.2$) is roughly spherical with radius $0.8h$.

(3) Direct information on *turbulence length scales and convection velocities* is also available from r_{ij}. The use of two-point data eliminates the uncertainties arising from the application of Taylor's hypothesis to single-point data, as in

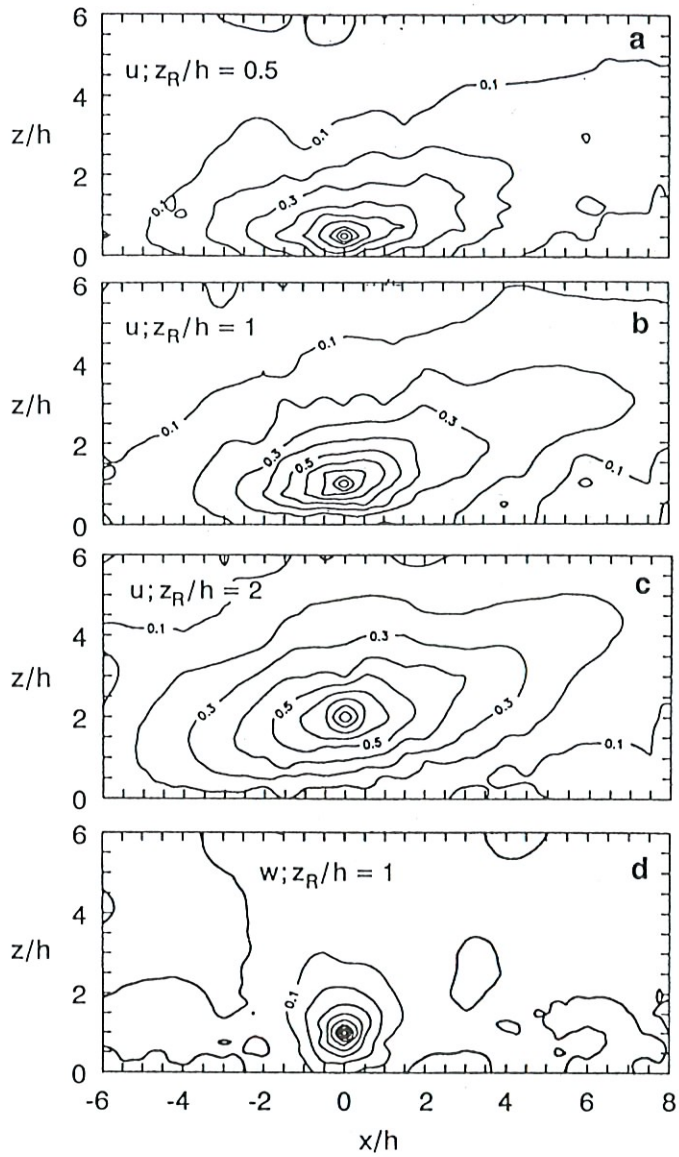

Figure 3. Spatial correlations at zero time delay, $r_{ij}(x, y, z, 0; z_R)$, for WT wheat (Table I) in the xz plane ($y = 0$). (a) u correlation (r_{11}) with $z_R/h = 0.5$; (b) r_{11} with $z_R/h = 1$; (c) r_{11} with $z_R/h = 2$; (d) w correlation (r_{33}) with $z_R/h = 1$. After Shaw *et al.* (1995).

Equation (1). Much better estimates of Eulerian length scales can be obtained by integration of the zero-time-delay r_{ij} along a streamwise transect:

$$L_i^{\cdot\cdot}(z) = \int_0^\infty r_{ii}(x, 0, z, 0; z)\, \mathrm{d}x \tag{4}$$

where the double dot superscript denotes the use of the two-point correlation. Shaw *et al.* (1995) used this equation to calculate $L_1^{\cdot\cdot} = L_u^{\cdot\cdot}$ and $L_3^{\cdot\cdot} = L_w^{\cdot\cdot}$ in the WT wheat canopy. Figure 5a compares these results with the single-point scales L_u and L_w from Equation (1) and Figure 1h,i. The single-point and two-point scales agree reasonably at heights well above the canopy, but progressively diverge with decreasing height. Within the canopy, the single-point L_u and L_w are each less

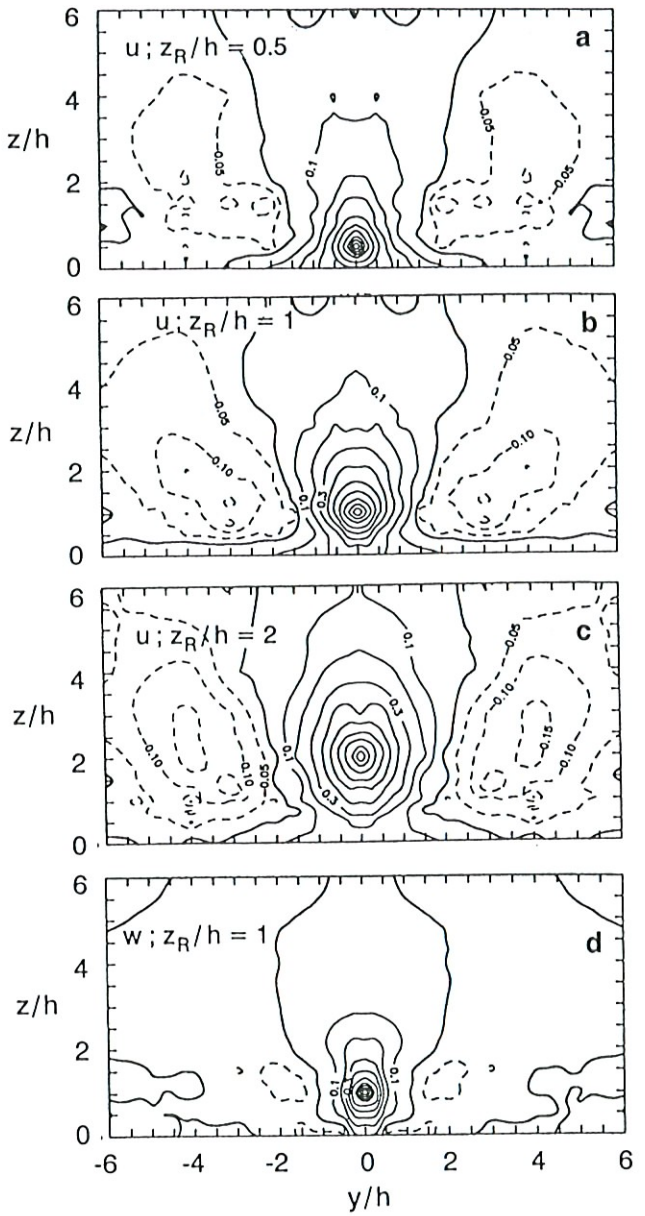

Figure 4. As for Figure 3, in the yz plane ($x = 0$). After Shaw *et al.* (1995).

than half their two-point counterparts. The reason is that, within and just above the canopy, the mean Eulerian velocity $U(z)$ is a poor estimate of the convection velocity $U_c(z)$ at height z. Shaw *et al.* (1995) estimated U_c in two ways: as $x/\tau_{\max}$ (where $\tau_{\max}$ is the time delay at which the correlation $r_{11}(x, 0, z, \tau; z)$ is maximum), and as UL_i^x/L_i, using the ratio of the two-point to single-point length scales. These estimates of U_c (Figure 5b) are significantly greater than U within and just above the canopy: at $z = h$, U_c is nearly $2U$. This agrees with visual observations of honami (Section 3.1), and with measurements of the translation speed of temperature microfronts in an almond orchard by Zhang *et al.* (1992).

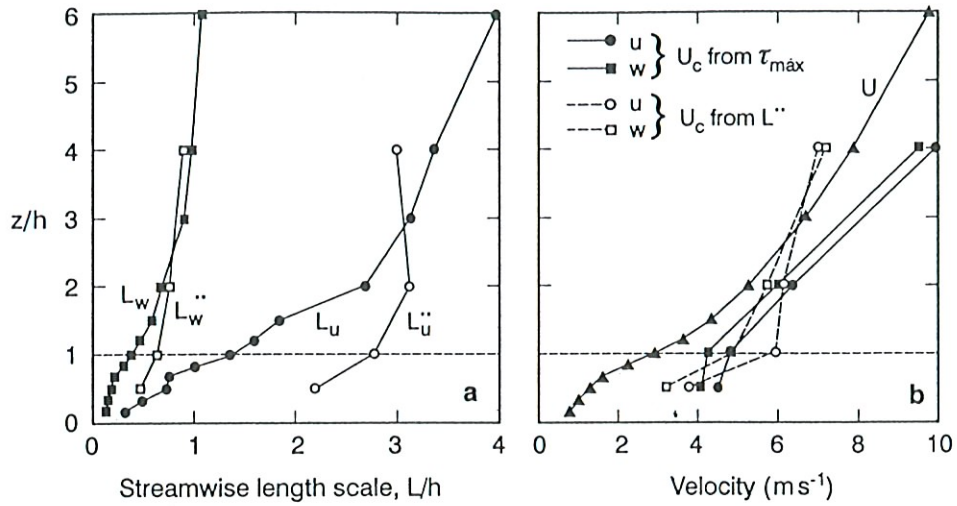

Figure 5. Two-point length scales $L_1^{\cdot\cdot} = L_u^{\cdot\cdot}$ and $L_3^{\cdot\cdot} = L_w^{\cdot\cdot}$ defined by Equation (4), and single-point length scales L_u and L_w, for WT wheat (Table I). (b) Convection velocities U_c, estimates as $x/\tau_{\max}$ and as $UL_i^{\cdot\cdot}/L_i$, compared with mean velocity $U(z)$. After Shaw *et al.* (1995).

3.3. CONDITIONAL ANALYSES

The term "conditional analysis" describes a broad class of methods (Antonia, 1981) for analysing one or more turbulence signals to extract information about postulated events or patterns of coherent motion. A "detector" or "condition" is used to identify realisations of the postulated event, and to assign each realisation a time origin such as the edge of a ramp structure. The realisations can then be averaged with aligned time origins to produce an ensemble-averaged pattern for the detected events. This can also lead to a determination of the contributions of these events to overall turbulent fluxes like $\overline{uw}$ and $\overline{w\theta}$. Several kinds of conditional analysis have been applied to canopy flows; these can be grouped into four categories according to the means of event detection.

(1) *Quadrant analysis* (Wallace *et al.*, 1972; Lu and Willmarth, 1973; Nakagawa and Nezu, 1977) was one of the earliest methods. Each instant of a $(u(t), w(t))$ record is classified as one of four kinds of "event" according to its quadrant in the uw plane, yielding the contribution of each quadrant to the overall momentum flux $\overline{uw}$. Of greatest importance are the ejection $(u < 0, w > 0)$ and sweep $(u > 0, w < 0)$ quadrants. Extensive applications to canopy data have shown that the ejection and sweep quadrants contribute about equally to $\overline{uw}$ in the inertial sublayer, but that sweeps dominate $\overline{uw}$ within the canopy (Finnigan, 1979a; Raupach, 1981; Shaw *et al.*, 1983; Coppin *et al.*, 1986; Baldocchi and Meyers, 1988a; Bergström and Högström, 1989). Through a cumulant expansion of the joint uw probability distribution (Nakagawa and Nezu, 1977), this result accords with the observed behaviours of Sk_u and Sk_w (Figure 1e,f) and the T_t term in the TKE budget (Figure 2). The contribution of quadrant analysis is therefore significant; however, the method says nothing about the spatial properties or characteristic flow patterns of the turbulence.

(2) *Visual event detection* is based on recognition of the ramp structures present in many turbulence signals (especially θ and u). Ramps are observed in the atmospheric boundary layer (Taylor, 1958; Priestley, 1959; Antonia *et al.*, 1979; Wilczak, 1984); in laboratory boundary layers (Chen and Blackwelder, 1978); and in vegetation canopies, especially forests (Gao *et al.*, 1989; Bergström and Högström, 1989; Paw U *et al.*, 1992). In canopies, the ramps often occur coherently through much of the canopy depth. Visual detection of these structures, followed by ensemble-averaging, has been used to construct pictures of the flow field around ramps (Wilczak, 1984; Bergström and Högström, 1989; Gao *et al.*, 1989).

(3) *Automated algorithms for detecting sharp changes in turbulence signals* have been developed with the aim of streamlining and removing subjectivity from visual ramp detection. These algorithms include Variable-Interval Time Averaging (VITA) (Blackwelder and Kaplan, 1976), Window-Averaged Gradient (WAG) (Bisset *et al.*, 1991), methods based on multilevel detection of sharp temperature drops (Shaw *et al.*, 1989; Paw U *et al.*, 1992), and a running-correlation method used by Qiu *et al.* (1995). All these methods require parameters, such as detection thresholds and window lengths, which are usually set by calibration against visually identified ramps. Hence, the methods remain subjective to some extent.

(4) *Event detection based on wavelet transforms* is an approach which offers more objectivity. For a signal $u(t)$, the wavelet transform is (Collineau and Brunet, 1993a):

$$W(a,b) = a^{-p} \int_{-\infty}^{\infty} u(t) g^{*}\left(\frac{t-b}{a}\right) \mathrm{d}t \tag{5}$$

where * denotes the complex conjugate, a is a "scaling" or "dilation" parameter, b a "time-translation" parameter, g is a "wavelet function" (vanishing at $\pm\infty$ and having a finite square integral), and the exponent p is usually chosen as 1. For given a, the wavelet transform produces a time-like record (in b) showing the extent to which the signal $u(t)$ "matches" the wavelet pattern g. The "wavelet spectrum" is the variance of this record as a function of a. This spectrum is typically fairly smooth, with a well-defined peak (at $a = a_p$) which objectively determines the mean duration of the events selected by the wavelet pattern.

Collineau and Brunet (1993a,b) and Brunet and Collineau (1994) outlined the application of wavelet transforms to canopy turbulence studies, offering four choices for the wavelet shape g: MHAT (a twice-differentiated Gaussian), WAVE (a once-differentiated Gaussian), HAAR (a single square wave cycle) and RAMP (a single sawtooth wave cycle). These can be classified according to whether detection of an event occurs when the transform $W(a,b)$ crosses zero on the time axis b, or exceeds some threshold. Wavelet shapes which are symmetric in time (MHAT) lead to zero-crossing event detection, whereas those antisymmetric in time (WAVE, HAAR, RAMP) lead to threshold detection. The particular transform $W(a_p,b)$ (in which a is set to the wavelet spectral peak a_p) is therefore an event detector requiring no calibration parameters for the MHAT wavelet, and one (threshold) parameter

for WAVE, HAAR and RAMP. Collineau and Brunet (1993b) compared these four wavelets, together with the VITA and WAG detection schemes, using four hours of summer, daytime data from Les Landes forest, Bordeaux. They found, first, that the MHAT event detector, $W(a_p, b)$, gave excellent agreement with visual ramp detection in determining the *number* (N) of ramp structures in a temperature record of duration T, thus providing an objective measure of the mean interval N/T between structures ($1.8h/u_*$ for their data). Second, the *location* of particular structures was determined best by RAMP, with the threshold parameter set by requiring that RAMP detect N structures. Brunet and Collineau (1994) obtained similar results in a maize canopy. Lu and Fitzjarrald (1994) carried out a wavelet analysis of a much larger data set from Harvard Forest, Massachusetts, using the HAAR wavelet applied to the θ signal. They obtained nearly identical conclusions to Collineau and Brunet (1993b), and also noted changes in N between day and night, and between summer and winter (leafless) conditions. We return to these results in Section 5.2.

4. The Mixing Layer

In the next two sections we turn to the proposal that turbulence and coherent motions near the top of the canopy are patterned on the flow in a plane mixing layer rather than a boundary layer. This section reviews some fluid-mechanical properties of the mixing layer.

4.1. Definition and basic properties

The ideal (plane, coflowing) mixing layer forms when two coflowing streams with different velocities, initially kept separate by a splitter plate, are allowed to mix (Figure 6). We let the splitter plate be in the horizontal half-plane $z = 0$, $x < 0$, with the flows in the $+x$ direction. The mixing layer becomes turbulent and then self-preserving as x increases, with a depth proportional to $x - x_0$, where x_0 is a virtual origin (Townsend, 1976, Section 6.10). The depth of the mixing layer can be quantified by the vorticity thickness $\delta_\omega = \Delta U/(\mathrm{d}U/\mathrm{d}z)_{\max}$, where ΔU is the difference between the two free-stream velocities; an alternative measure, the momentum thickness δ_m, is typically about $\delta_\omega/4.5$, depending slightly on the shape of $U(z)$ (Rogers and Moser, 1994).

Figure 7 shows several observed properties of the fully-developed, self-preserving mixing layer. Velocity moments show a strong inflection in $U(z)$ at the centreline (Figure 7a), and single peaks in $\overline{uw}$, σ_u and σ_w (Figure 7b). Near the centreline, $\sigma_u/u_* \approx 1.7$, $\sigma_v/u_* \approx 1.5$, $\sigma_w/u_* \approx 1.3$ and $r_{uw} \approx -0.44$ (defining u_* for the mixing layer as $\max(-\overline{uw})^{1/2}$). There are antisymmetric double peaks in Sk_u and Sk_w (Figure 7d) which indicate that momentum transfer is dominated by sweeps on the low-velocity side of the flow and by ejections on the high-velocity

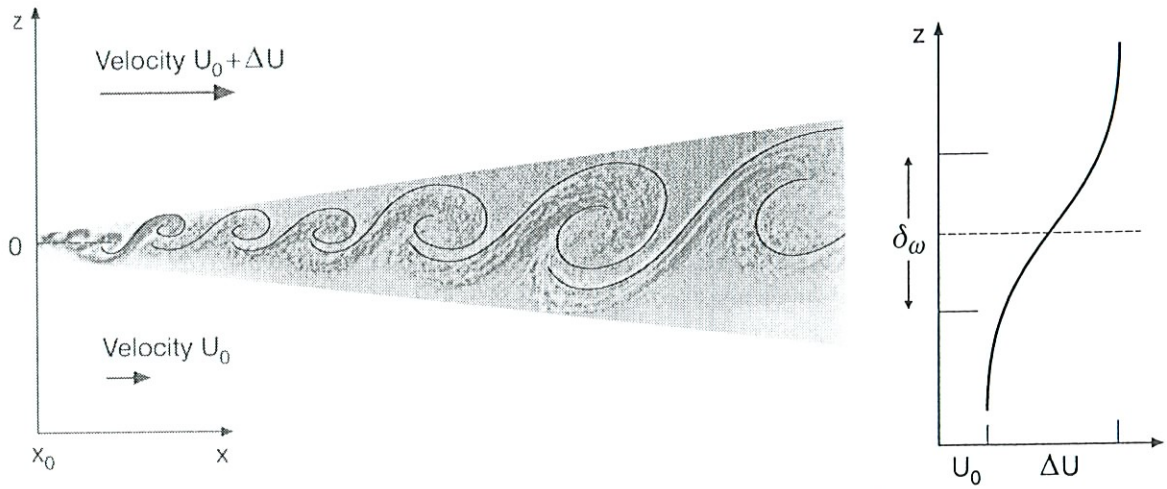

Figure 6. The plane mixing layer, showing the vorticity thickness δ_ω.

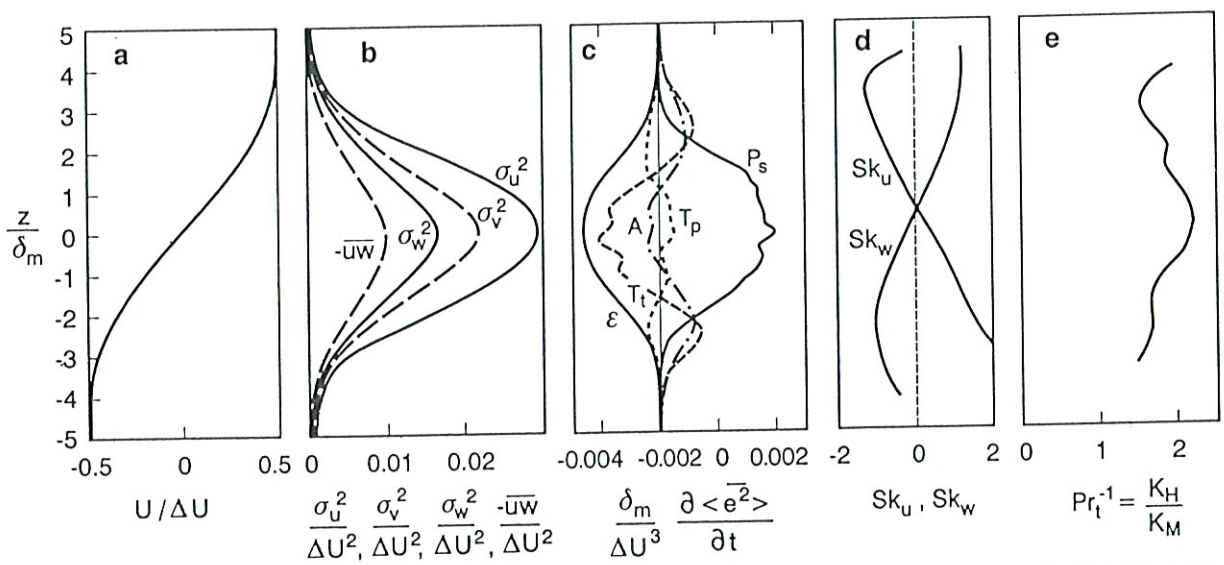

Figure 7. Flow statistics in the self-preserving region of a plane mixing layer, normalised with ΔU and momentum thickness δ_m: (a) U; (b) σ_u, σ_w and $\overline{uw}$; (c) TKE balance (terms as in Equation (2) except for time derivative term, A); (d) Sk_u and Sk_w; (e) inverse turbulent Prandtl number $\mathrm{Pr}_t^{-1} = K_H/K_M$. Sources of data: (a), (b) and (d) compiled from Wygnanski and Fiedler (1970) and Bell and Mehta (1990); (c) from DNS results for a temporally-growing mixing layer by Rogers and Moser (1994); (e) calculated by present authors from data of Fiedler (1974) on $U(z)$ and $\Theta(z)$ in a mixing layer with one slightly heated stream, using conservation and self-preservation assumptions.

side, in the terminology of quadrant analysis. The turbulent energy budget (Figure 7c) is characterised by strong turbulent transport away from the zones of highest shear production into the low-production regions, and is far from local equilibrium condition $P_s \approx \varepsilon$. The inverse turbulent Prandtl number $\mathrm{Pr}_t^{-1} = K_H/K_M$ is around 2 in a mixing layer (Figure 7e), a value typical of free shear flows including wakes and jets as well as mixing layers (Townsend, 1976). Table II summarises these statistical flow properties, comparing a mixing layer with a surface layer (the inertial sublayer of a neutral boundary layer).

Mixing-layer turbulence has a distinctive pattern of coherent motion, identified in the classic experiments of Brown and Roshko (1974) and by many subsequent

Table II

Comparison of statistical flow properties for a surface layer (inertial sublayer of a turbulent boundary layer); a mixing layer; and canopy flow near $z = h$. P, T and ε are respectively the production, transport and dissipation terms in the TKE budget, Equation (2).

Property	Surface layer	Mixing layer	Canopy ($z = h$)
$U(z)$ inflection	No	Yes	Yes
σ_u/u_*	2.5	1.7	1.8
σ_w/u_*	1.25	1.3	1.1
$r_{uw} = \overline{uw}/(\sigma_u\sigma_w)$	−0.32	−0.44	−0.5
$\mathrm{Pr}_t^{-1} = K_H/K_M$	1.1	2	2
$\lvert\mathrm{Sk}_u\rvert$, $\lvert\mathrm{Sk}_w\rvert$	Small	O(1)	O(1)
u, w	$\propto z - d$	$\propto \delta_\omega$	$\propto h - d$
TKE budget	Small T: $0 \approx P - \varepsilon$	Large T: $0 = P + T - \varepsilon$	Large T: $0 = P + T - \varepsilon$

workers. Flow visualisations and other techniques reveal a strong, large-scale coherent motion consisting of a series of primarily transverse vortices. The streamwise periodicity or separation between vortices, Λ_x, increases with mixing-layer depth δ_ω. Both are proportional to $x - x_0$ in the self-preserving region. Experimental and numerical determinations of Λ_x/δ_ω in this region are in the range 3.5 to 5 (Dimotakis and Brown, 1976; Rogers and Moser, 1994).

4.2. Hydrodynamic stability theory

A starting point for the analysis of mixing-layer development is offered by classical, linear, Hydrodynamic Stability Theory (HST). The approach is to consider weak oscillatory perturbations, or modes, embedded in an otherwise laminar shear flow with background velocity profile $U(z)$. A given mode may decay, amplify or remain steady in time. The analysis uses linearised dynamical equations to identify the possible modes, determine their development, and in particular to find the wavenumbers, phase speeds and initial growth rates of the amplified modes, since ultimately these dominate. Reviews are given by Monin and Yaglom (1971) and Drazin and Reid (1981). We are concerned here with the stability properties of a plane shear flow with an inflection in $U(z)$. The basic instability in this flow is caused by inviscid effects, with viscosity playing only a minor damping role (Betchov and Criminale, 1967); it is therefore sufficient to consider the inviscid problem. It is also sufficient to study the two-dimensional (x, z) problem, because for any three-dimensional mode, there exists a corresponding, faster-growing two-dimensional mode (Squires' theorem in the inviscid case). The classical approach is to consider the perturbation stream function $\psi(x, z, t)$, letting $(u, w) = (\partial\psi/\partial z, -\partial\psi/\partial x)$ be a small perturbation in the two-dimensional

velocity vector about the background velocity $(U(z), 0)$. Solutions are sought in the form

$$\psi(x, z, t) = \phi(z) \exp(i(kx - \omega t)) = \phi(z) \exp(ik(x - ct)) \tag{6}$$

which represents a single mode as a wave propagating in the x direction with wavenumber k, angular frequency ω, phase velocity $c = \omega/k$ and amplitude $\phi(z)$. The problem is governed by the Rayleigh equation, an equation for ϕ derived from the linearised, inviscid momentum equation:

$$(U - c)(\phi'' - k^2\phi) - U''\phi = 0 \tag{7}$$

with $\phi = 0$ on the boundaries. The double primes denote double z derivatives. This is an eigenvalue problem with nontrivial solutions $\phi(z)$ (eigenmodes) only for certain values of c (eigenvalues) which depend on k. A given mode is possible if $c = \omega/k$ is an eigenvalue of Equation (7); it is then stable, neutral or unstable if $\mathrm{Im}(c)$ is negative, zero or positive, respectively. Theorems due to Rayleigh and Fjørtoft (see Drazin and Reid, 1981) show that a necessary condition for the existence of unstable modes is that $U(z)$ has an inflection point where U' is maximum, like the mixing-layer $U(z)$ in Figure 7a. The unstable modes generate two-dimensional waves known as transverse Kelvin-Helmholtz (KH) waves; these constitute an entire family of motions which emerge in a laminar mixing layer but not in a laminar boundary layer, because the mixing layer has an inflectional $U(z)$ (with maximal U') but the boundary layer does not.

Michalke (1964, 1965) calculated the unstable modes in a parallel-flow mixing layer with the unperturbed velocity profile

$$U(z)/U_s = 1 + \tanh(z/L_s) \tag{8}$$

where $L_s = \delta_\omega/2$ and $U_s = \Delta U/2$. For this velocity profile, $\delta_\omega = 4\delta_m$. The analysis shows that the unstable modes are those with $0 < kL_s < 1$. In the temporal case (homogeneous in x but evolving in time) the fastest-growing mode is $kL_s = 0.4446$ or $\Lambda_x/L_s = 14.13$, where $\Lambda_x = 2\pi/k$ is the streamwise wavelength of the KH waves; in the spatial case (steady in time and evolving in x) it is $kL_s = 0.4031$ or $\Lambda_x/L_s = 15.59$. The precise shape of the $U(z)$ profile does not have a strong influence, as shown by similar calculations with a piecewise-linear $U(z)$ (Drazin and Reid, 1981, p. 146). The results for the spatial case are in good agreement with observations of both the spacings and growth rates of the transverse vortices in the early stages of the growth of a mixing layer (Ho and Huerre, 1984).

4.3. Development towards the fully turbulent state

Because of its linearity, HST ceases to apply as soon as the instabilities grow to a finite size, which happens very quickly. The subsequent nonlinear development

of the mixing layer towards a fully turbulent state includes several additional instability processes, reviewed by Ho and Huerre (1984), for example. These have been studied experimentally, analytically and numerically, including recent Direct Numerical Simulation (DNS) studies by Comte *et al.* (1992) and Rogers and Moser (1994); the latter achieves high enough Reynolds numbers to reach the fully turbulent, self-preserving state.

The development sequence includes the following processes. First, the transverse vorticity in the KH waves quickly "rolls up" under a nonlinear self-interaction into a string of concentrated "rollers", separated by "braid regions" in which the transverse vorticity is lower but the strain rate is higher. The roller regions are dominated by rotation and the braid regions by strain (Rogers and Moser, 1994). Next, three-dimensional instabilities lead rapidly to the development of longitudinal vorticity, in the form of "braid" or "rib" vortices in the highly-strained braid regions (Pierrehumbert and Widnall, 1982). Third, and at the same time, neighbouring transverse vortex rollers begin to amalgamate under a stochastic "pairing" process (Winant and Browand, 1974), introducing irregularities into the spacing between rollers. Fourth, after (typically) two or three vortex pairings, a distinct "mixing transition" occurs, corresponding to the initiation of fully developed, three-dimensional turbulence (Dimotakis and Brown, 1976). Finally, a short time later, the turbulence assumes a self-preserving form. By this stage, vortex amalgamation appears to be dominated not by pairing but rather by "tearing", the destruction of a transverse vortex and engulfment of its vorticity by the strain field of its neighbours (Moore and Saffman, 1975; Rogers and Moser, 1994). The long transverse rollers which are evident prior to the mixing transition are less organised after transition, with amalgamations apparently occurring stochastically in the xy plane, leading to "branchings" of the transverse rollers (Browand and Troutt, 1980; Comte *et al.*, 1992). The region of strong two-point velocity correlation at zero time delay ($r_{11} > 0.2$) extends about $\pm 2\delta_m \approx \pm\delta_\omega/2$ in the streamwise direction, and $\pm 6\delta_m \approx \pm 1.5\delta_\omega$ in the transverse direction (Browand and Troutt, 1980).

Observed values of Λ_x/δ_ω in a fully turbulent mixing layer are between 3.5 and 5. These are consistent with the theoretical criterion $\Lambda_x/\delta_\omega < 3.5$ for the amalgamation by tearing of a linear array of transverse vortices (Moore and Saffman, 1975), but are less than the fastest-growing KH wavelength predicted from linear HST in the spatial case (Michalke, 1965), for which $\Lambda_x/\delta_\omega = \Lambda_x/(2L_s) = 7.8$. Nevertheless, HST may retain some conceptual applicability even for the fully developed shear layer, if the large coherent motions are regarded as "instabilities propagating on a flow defined by the time-averaged velocity field" with the smaller-scale turbulence providing an (eddy) viscosity (Ho and Huerre, 1984, p. 387). There are several possible reasons for the difference between observations and HST predictions of Λ_x/δ_ω: (1) the mixing layer is growing linearly ($\delta_\omega \propto x - x_0$) in the observations, but δ_ω is constant with x in the analysis; (2) there is additional entrainment in a high Reynolds number mixing layer caused by the fine-scale turbulence, which causes an increase in $\mathrm{d}\delta_\omega/\mathrm{d}x$ at mixing transition; and (3) most importantly,

nonlinearities cause the emergence of modes other than the fastest-growing KH mode, as suggested by the DNS study of Comte *et al.* (1992).

Both experimental and numerical studies have shown that the exact development and properties of a mixing layer are sensitive to initial conditions: for example, whether the splitter plate boundary layers are laminar or turbulent, or periodic forcing of the mixing layer in its initial stages (Ho and Huerre, 1984; Rogers and Moser, 1994). This indicates that mixing layers "forget" their initial conditions extremely slowly (Dimotakis and Brown, 1976). Nevertheless, the above description applies generically to mixing layers without initial forcing.

5. The Mixing-Layer Analogy for Canopies

An analogy between turbulent flow in a mixing layer and near the top of a canopy is suggested initially by the inflectional mean velocity profile $U(z)$ in both flows. Several consequences follow if the analogy is accurate: the values of statistical flow properties such as $\sigma_{u,v,w}/u_*$, r_{uw} and K_H/K_M in canopy turbulence should be closer to typical values in a mixing layer than a surface layer (the inertial sublayer of a thermally neutral turbulent boundary layer); the turbulent energy budget in a canopy should approximate that in a mixing layer; and the dominant length scales of canopy turbulence should also be predictable from those observed in mixing layers. The extent to which these expectations are satisfied constitutes a series of tests of the hypothesis.

5.1. Tests based on statistical flow properties

The material presented so far has shown that many properties of canopy flow are indeed closer to mixing-layer than surface-layer values. Table II compares several flow properties between a surface layer, a mixing layer and typical canopy flow near $z = h$. In particular, σ_u/u_* is around 30% lower, and $|r_{uw}|$ is 30% higher, in both the canopy and the mixing layer compared with the surface layer. The u and w skewnesses are both significant (around 1 in peak absolute value) in the mixing layer and the canopy, but are small in the surface layer. The signs of Sk_u and Sk_w imply that momentum transfer is dominated by sweeps ($u > 0, w < 0$) on the low-velocity side of the mixing layer, as in the canopy. The turbulent energy budget is far from local equilibrium in both the mixing layer and the canopy (turbulent transport being comparable with production in both flows) but is close to local equilibrium in the surface layer. The eddy diffusivity ratio K_H/K_M is around 2 in the core of the mixing layer and in canopy flow just above $z = h$, but is about 1.1 in the surface layer.

Rapid Distortion Theory (RDT), reviewed by Townsend (1976), Savill (1987) and Hunt and Carruthers (1990), offers some explanation for the differences in statistical flow properties between mixing layers and boundary layers, and thence

for the behaviour of these properties in canopy flow near $z = h$. RDT uses the linearised equations of motion to calculate what happens to an initially specified turbulent velocity field under various kinds of mean-flow distortion, specified in our case by $U(z)$. In this respect RDT differs from HST (another linearised theory), which seeks the fastest-growing eigenmodes or resonant modes of the flow. Mathematically, the flow equations (for instance the Rayleigh equation (7)) can support both a discrete spectrum of exponentially growing ($\mathrm{Im}(c) > 0$) or decaying ($\mathrm{Im}(c) < 0$) eigenmodes, and a continuous spectrum of neutral eigenmodes ($\mathrm{Im}(c) = 0$) which do not grow or decay exponentially with time (Drazin and Reid, 1981); HST studies the discrete eigenmodes, while RDT deals with the continuous spectrum of neutral eigenmodes.

A simple and important case is that of uniform shear, $U(z) = \alpha z$ with a constant rate of strain $\alpha = \mathrm{d}U/\mathrm{d}z$. The RDT solution for initially isotropic turbulence was obtained by Townsend (1970, 1976), and for initially axisymmetric turbulence by Maxey (1982). The solution yields predictions of the two-point covariance $R_{ij}(\mathbf{r}, t) = \overline{u_i(\mathbf{x}, t)u_j(\mathbf{x} + \mathbf{r}, t)}$, ratios among the Reynolds stress components $\overline{u_i u_j}$, and the inverse turbulent Prandtl number K_H/K_M (all as functions of the dimensionless total strain $\beta = \alpha t$, where t is the distortion time). The predictions strongly resemble observations in real turbulent shear flows; for instance, the predictions for $R_{ij}(\mathbf{r}, t)$ (Townsend, 1970) match observations by Grant (1958) in eight out of nine tensor components, and also include the main features of our own R_{ij} measurements (Figures 3, 4). This is remarkable in view of the extreme simplifications of the theory, which include linearisation, homogeneity, and *ad hoc* specification of the initial turbulence. In particular, RDT yields reasonable predictions of several turbulence properties for both a mixing layer and a surface layer, provided that different total strains are chosen for each: $\beta \approx 2$ for a mixing layer and $\beta \approx 5$ for a surface layer. In effect, β is calibrated against one turbulence property, other properties then being independent predictions. Table III shows the RDT predictions for σ_u/u_* and K_H/K_M at these β values. There is a general (though not exact) correspondence with the mixing-layer values from Table II at $\beta = 2$, and the surface-layer values at $\beta = 5$. This suggests that, within the limits of its assumptions, RDT does indeed capture the main statistical properties of shear flows, and that the statistical differences between the mixing layer and the surface layer are associated with differing values of the effective total strain in each flow.

5.2. Tests based on turbulent length scales

Of several possible turbulent length scales, we focus on Λ_x, the mean streamwise periodicity or x-distance between successive coherent eddies. A prediction for Λ_x in canopy flow near $z = h$ can be made by recalling two estimates of Λ_x for the mixing layer: HST predicts $\Lambda_x/\delta_\omega = 7.8$ for the fastest-growing KH spatial wave, while experiments and DNS results for fully-developed mixing layers give

Table III
Predictions of Rapid Distortion Theory (RDT) for two values of total strain β, from Townsend (1976, Figure 3.15, case $N = 0$, and Figure 8.4)

β	2	5
σ_u/u_*	1.71	2.23
K_H/K_M	1.9	1.4

$\Lambda_x/\delta_\omega \approx 3.5$ to 5. Of these, the fully-developed value is more relevant to canopies. To estimate δ_ω for the canopy mixing layer, we consider

$$L_s = U_h/U_h' = U(h)/(\mathrm{d}U/\mathrm{d}z)_{z=h} \tag{9}$$

which is a basic shear length scale for canopy flow. This is equal to $\delta_\omega/2$, under two modest assumptions: (1) the inflection point in $U(z)$ is at $z = h$ (which can be regarded as a definition of h!); and (2) $U_0 \ll U_h$, where U_0 is the velocity on the low-speed side of the canopy mixing layer, or the velocity in the low-shear region deep within the canopy. Taking Λ_x/δ_ω in the range 3.5 to 5 and $\delta_\omega = 2L_s$, we obtain the prediction

$$\Lambda_x = mL_s = mU_h/U_h' \tag{10}$$

where m is in the range 7 to 10. This prediction can be tested in four ways.

(1) The *spectral peak frequency* f_p is related to Λ_x by $\Lambda_x = U_c/f_p$, where U_c is the convection velocity. It is appropriate to use the w spectrum for this purpose, since it reflects the active turbulence near $z = h$ which induces the primary vertical motions and mediates the vertical transfer of momentum and scalars. In contrast, the u and θ spectra include contributions from inactive turbulence, the larger-scale quasi-horizontal motions in the surface and canopy layers which modulate the active turbulence near $z = h$ but do not contribute significantly to vertical transfer (Bradshaw, 1967; Townsend, 1976; Perry *et al.*, 1986). We expect the active turbulence, but not the inactive turbulence, to be dominated near $z = h$ by inflectional instability processes, and therefore to be described by the mixing-layer analogy. Using the peak frequency $f_{p(w)}$ of the w spectrum, we obtain the estimate

$$\frac{\Lambda_x}{h} = \frac{U_c}{f_{p(w)}h} = \left(\frac{U_h}{f_{p(w)}h}\right)\left(\frac{U_c}{U_h}\right). \tag{11}$$

For a "generic" canopy, $f_{p(w)}h/U_h \approx 0.45$ below about $2h$, nearly independent of height (Section 2.2). Taking $U_c/U_h \approx 1.8$ near $z = h$, from evidence in Section

3.2, Equation (11) gives $\Lambda_x/h \approx 4$ as an "observed" value inferred from w spectral peak frequencies. This is in agreement with the prediction of Equation (10): taking $m = 8$ and $L_s/h = 0.5$ as a "generic" value from Table I, Equation (10) also gives $\Lambda_x/h \approx 4$.

(2) *Turbulence length scales derived from velocity correlations* offer a much more precise test, because canopy-specific, rather than generic, data are available. As with spectral peak frequencies, it is appropriate to use the length scale for w because this represents the active turbulence. Avoiding Taylor's hypothesis, the best estimate of Λ_x is obtained from the two-point length scale, as $\Lambda_x = 2\pi L_w^{..}$. Here the factor 2π relates the decay or correlation length scale of the spatial signal $w(x)$ to the length scale for periodicity. Since the single-point scale L_w is much more widely available than $L_w^{..}$, we express Λ_x in terms of L_w rather than $L_w^{..}$, writing

$$\frac{\Lambda_x}{h} = 2\pi \left(\frac{L_w(h)}{h}\right)\left(\frac{U_c}{U_h}\right) \tag{12}$$

where L_w is evaluated at $z = h$, and the factor U_c/U_h converts U_h in Equation (1) to the convection velocity.

Figure 8 plots the observed length scale Λ_x obtained from Equation (12) against the shear length scale $L_s/h = U(h)/(hU'(h))$, for the canopies in Table I (L_w data were not available in two cases). We have assumed $U_c/U_h = 1.8$ throughout, following Section 3.2. For all canopies, covering a 10-fold range in L_s/h and a 400-fold range in h, the points lie close to a straight line of slope $m = 8.1$. This provides strong evidence that the length scales of active turbulence near the top of a canopy are controlled by the shear length scale $L_s = U(h)/U'(h)$, and also that the proportionality between the periodicity Λ_x and L_s is the same as in a mixing layer.

Figure 9 shows the normalised single-point turbulence length scales $L_u(h)/h$ and $L_w(h)/h$ (evaluated at $z = h$), plotted against L_s/h. The values of L_w fall very close to a straight line ($L_w = 0.71L_s$) consistent with Figure 8, while those of L_u are much more scattered. This reinforces the view that vertical velocities near $z = h$ are dominated by active turbulence which scales with L_s, while horizontal velocities include contributions from larger-scale, quasi-horizontal eddies which do not scale on local canopy length scales such as L_s, but rather on larger length scales such as the overall boundary-layer depth.

(3) *Wavelet analysis* enables Λ_x/h to be estimated as $(T/N)(U_c/h)$, where N is the number of structures detected in time T. It is important to note that N, and therefore the inferred Λ_x/h, depend on the variable used for structure detection (u, θ or w). Table IV shows results for all three variables, obtained from Les Landes forest (Collineau and Brunet, 1993b) and a maize canopy (Brunet and Collineau, 1994). These values were recomputed for the present paper from the original raw data. They show that values of Λ_x/h inferred from u, θ and w are in the approximate ratio 3 (u) to 1.7 (θ) to 1 (w), for near-neutral data. Detection frequencies N/T

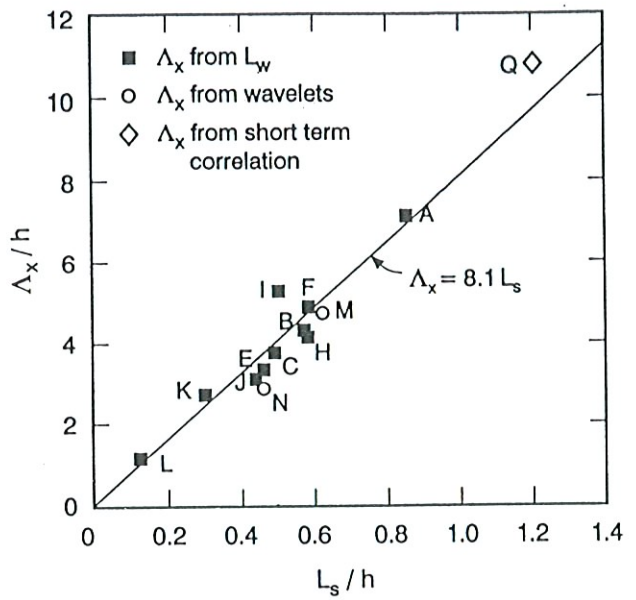

Figure 8. Periodicity (mean streamwise separation) Λ_x of active eddies near $z = h$, plotted against shear length scale $L_s = U(h)/U'(h)$. Both axes are normalised with h. For canopies A to L (Table I), Λ_x is estimated from $L_w(h)$ using Equation (12). For canopies M and P (Les Landes forest and Brunet maize: Table IV), Λ_x is estimated from wavelet event detection on w signal. For canopy Q (wheat: Finnigan 1979a,b), Λ_x is estimated from short-term two-point u correlations. Straight line is $\Lambda_x = mL_s$ with m = 8.1. Both axes are normalised with canopy height h.

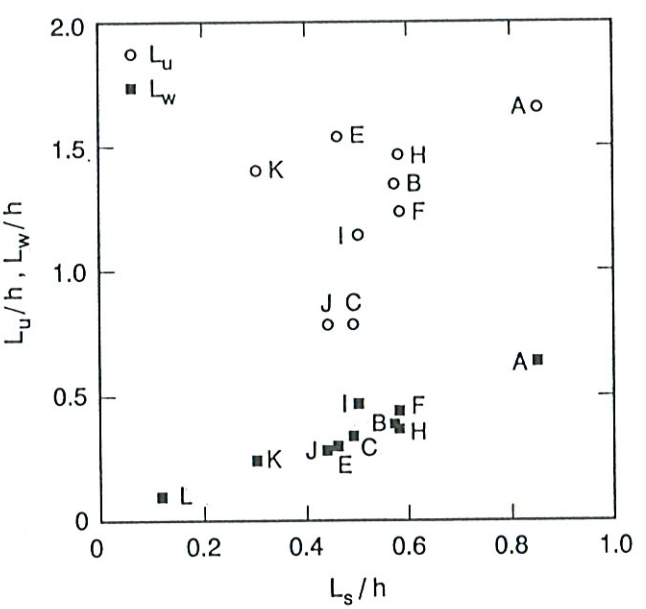

Figure 9. Single-point length scales at $z = h$, $L_u(h)$ and $L_w(h)$, plotted against shear length scale $L_s = U(h)/U'(h)$, for canopies A to L (Table I). Both axes are normalised with canopy height h.

for the three variables are in the inverse ratio, 0.3 to 0.6 to 1. These ratios are, not coincidentally, quite close to those for spectral peak frequencies (Section 2.2).

Consistent with the tests using spectral peak frequencies and turbulence length scales, we use the wavelet analysis for w to estimate Λ_x/h. The data in Table IV then yield two additional pairs of $(L_s/h, \Lambda_x/h)$ values: (0.62, 4.7) for Les Landes

Table IV

Wavelet analysis results for streamwise separation between structures in u, θ and w records from three canopies, estimated as $\Lambda_x/h = (T/N)(U_c/h)$ where N is number of structures detected in time T. Results for canopies M and N calculated from original raw data by M. R. Irvine and Y. Brunet, using MHAT and $U_c/U_h = 1.8$. Results for canopy P from Table III in Lu and Fitzjarrald (1994), assuming $U_c = U(z = 1.5h)$.

Canopy	Ident	$TU_c/N_u h$	$TU_c/N_\theta h$	$TU_c/N_w h$	L_s/h	Reference
Les Landes forest (near-neutral)	M	12.1	8.0	4.7	0.62	Collineau and Brunet (1933b)
Maize:						
near-neutral:	N	10.0	5.1	2.8	0.46[a]	Brunet and
slightly stable:		9.3	2.1	2.0	–	Collineau (1994)
Harvard forest						
summer:	P	–	12.7	–	–	Lu and
winter:		–	14.8	–	–	Fitzjarrald (1994)

[a] Value for canopy E in Table I, a canopy of similar species and leaf area index.

forest, and (0.46, 2.8) for daytime maize (here the L_s/h value is "borrowed" from the structurally very similar canopy E). These data are superimposed on Figure 8 as points M and N, with excellent agreement.

Table IV also shows results by Lu and Fitzjarrald (1994) from Harvard forest, using θ for detection. They found systematic variations of Λ_x/h with time of day and with season, such that Λ_x/h is larger in daytime than nocturnal conditions and in winter than in summer. The variation with time of day is confirmed by the maize data in Table IV. These variations are consistent with Equation (10), since L_s/h is expected to be higher in daytime than nocturnal conditions, and higher in winter (leafless) than summer (fully leaved) conditions.

Paw U *et al.* (1992) and Qiu *et al.* (1995) report somewhat different analyses of turbulence data from forest (h = 18 m), orchard (h = 6 m) and maize (h = 2.6 m) canopies. The former study used a method based on multilevel detection of sharp temperature drops. The latter used a "pseudo-wavelet" method based on a calibrated running-correlation detection scheme, which does not exploit the full frequency properties of a wavelet analysis. Both studies found that Λ_x/h was around 10 for forest, but for lower canopies, the arrival frequency $f = U_c/\Lambda_x$ of the detected structures approached a constant value (0.02 Hz) with increasing U_h/h. This apparently contradicts the prediction of Equation (10) that $U_c/\Lambda_x = U_c/mL_s \propto U_h/h$ (assuming $U_c \propto U_h$ and $L_s \propto h$). A probable interpretation is that the detected structures are not the same as the active turbulence discussed above. For the active turbulence, Figures 8 and 9 show that L_w and Λ_x are both proportional to L_s. A detection frequency f independent of L_s implies that the detection algorithm responds to turbulence structures which scale on lengths other than L_s, presumably the outer layer length scales associated with inactive turbulence near $z = h$. The

"signal-to-noise" ratio of such a detection scheme might therefore be good over the forest but lower over shorter canopies, where there is more inactive turbulence as argued at the end of Section 6. This would cause the detection scheme to miss events over the lower canopies.

(4) *Observations of periodicity in short-term correlations* provide a different test. Periodicity in long-term single-point u correlations is observed in a mixing layer (Dimotakis and Brown, 1976) but not in a surface layer (Townsend, 1976), where the long-term correlation smears out many quasi-periodic events with a range of frequencies. Similar smearing is expected in canopy flow (see concluding discussion); therefore, any periodicity associated with coherent eddies of the mixing-layer type should be much more evident in short-term than long-term correlations from canopies. Moreover, this periodicity should be evident at similar frequencies in both the u and w correlations (r_{11}, r_{33}), because the active turbulence associated with mixing-layer coherent eddies involves all velocity components.

The only observations of short-term correlations available to us are by Finnigan (1979a,b). As part of a study of *honami* waves, he measured short-term, two-point u correlations $r_{11}(0, 0, z, \tau; z_R)$ in a sparse wheat canopy with $h = 1.25$ m, roughness density $\lambda = 0.52$, and shear length scale $L_s/h = 1.2$. From two examples of strongly periodic short-term correlations (1979b, Figure 14), the dominant frequency f is at $U_h/fh = 6 \pm 1$. Estimating Λ_x/h as $(U_h/fh)(U_c/U_h)$ and taking $U_c/U_h = 1.8$ again, we obtain $\Lambda_x/h \approx 10.8$. This result is plotted in Figure 8 as point Q. It agrees very well with Equation (10) and with the other data, and also provides a valuable extrapolation to a very sparse (large L_s/h) canopy.

In summary, we have 10 measurements of Λ_x from turbulence length scales, two from wavelet analysis and one from short-term correlation periodicity, each with an associated value of L_s. Over these 13 data points, the average value of $m = \Lambda_x/L_s$ is 8.1 (standard deviation 1.1, standard error 0.3). This is in remarkable agreement with the *a priori* expectation from the mixing-layer analogy that m is in the range 7 to 10.

6. A Physical Picture, Discussion and Conclusions

The mixing-layer analogy suggests the following physical picture for the dominant eddy structure in a plant canopy. First, $L_s = U_h/U_h'$ is identified as the vertical length scale for the active canopy turbulence associated with strong vertical transfer. This scale is around $0.1h$, $0.5h$ and h for dense, moderate and sparse canopies, respectively. It is useful to distinguish three ranges of eddy scale: eddies much larger than L_s (inactive turbulence), comparable with L_s (active turbulence) and much smaller than L_s (fine-scale turbulence). At the largest scale, the canopy is immersed in a deep planetary boundary layer, usually a convective boundary layer by day. This boundary layer is dominated in its outer part by eddies scaling with the entire boundary-layer depth δ, and in its surface layer by eddies scaling with $z - d$.

All these eddies are "attached" in the sense that they make significant contributions to the overall turbulent velocity field near the surface (Townsend, 1976). However, the velocity fields of eddies which are much larger than h in vertical scale are practically horizontal at heights of order h, because of the constraints of continuity and the ground surface. Therefore, eddies with vertical length scales much greater than h (or L_s, which is of order h) can contribute little to vertical transfer, and constitute inactive turbulence at heights of order h. Their main effect in the canopy is to make the active, canopy-scale eddies intermittent.

The active, canopy-scale eddies are of order L_s in vertical scale and with streamwise separations $\Lambda_x = mL_s$, with $m = 8.1 \pm 0.3$ (Equation (10) and Figure 8). They originate from instabilities of the kind found in mixing-layer turbulence, associated with the inflection in the canopy velocity profile established by drag below $z = h$. The instabilities are patterned after the KH waves which emerge from linear HST in a flow with inflectional $U(z)$, but are modified from the KH form by several high-Reynolds-number processes including three-dimensional instabilities, nonlinear vortex interactions, and background small-scale turbulence which acts as an eddy viscosity. Nevertheless, the KH instabilities give a first indication of the length scale (Λ_x) of the main coherent motions at canopy scale.

The fine-scale turbulence ($\ll L_s$) is created both by the eddy cascade process and by wake shedding. It contributes little to vertical transfer, and is important mainly for its role in dissipating turbulent energy and providing an eddy-viscous drag on the larger eddies. The limited dynamical role of this turbulence is the main reason why the small-scale, three-dimensional details of canopy morphology have a negligible effect on turbulent transfer in reasonably dense canopies (as shown by the similarity of the turbulence in all the canopies in Figure 1). Rather, the role of the canopy elements is to create a vertically distributed momentum sink which sets up an inflectional velocity profile with length scale L_s, leading to dominant canopy eddies of this scale. However, in sparse canopies (where the plant spacing is of order h or larger) the velocity field becomes three-dimensional on the scale of L_s itself, leading to a more complicated picture.

We return to the effects of the intermittency of the large-scale, inactive turbulence. Because the growth rates of the mixing-layer instabilities are proportional to the shear U_h' at $z = h$, faster growth and larger-amplitude instabilities arise during large-scale gusts than during large-scale lulls. The effect is accentuated by the proportionality of the canopy drag to U^2 rather than U, which causes U_h' to increase faster than linearly with U. Consequently, large-scale gustiness modulates the canopy-scale coherent motions. Each large-scale gust initiates a "wave packet" of several canopy-scale coherent motions with streamwise periodicity $\Lambda_x \approx 8L_s$. These motions are very effective at scalar and momentum transfer, and thus rob the large-scale gust of its momentum and eventually destroy it. This is the likely reason that *honami* waves and canopy-scale sweeps (the motions dominating canopy momentum transfer) tend to occur in groups of three or four (Finnigan, 1979a,b). Also, the streamwise spacing and therefore the short-term periodicity

of the canopy-scale coherent motions within each large-scale gust varies from instance to instance; this leads to strong periodicities in short-term velocity correlations (Finnigan, 1979b) which are smeared out in longer-term correlations by averaging over multiple frequencies, giving aperiodic long-term correlations as observed.

In the above discussion we have been rather severe in the distinction between inactive, active and fine-scale turbulence. In practice, these categories merge into a continuous spectrum, in which different wavenumber ranges obey different scaling laws (Perry *et al.*, 1986). One potentially important modification to the conventional distinction between inactive and active turbulence (e.g. Townsend, 1976) is that a canopy is porous below its mean level of momentum absorption; therefore, continuity constraints on vertical transfer by large eddies are not as severe as for an impervious wall. The extent to which large eddies become involved in active transfer will therefore increase as the ratio h/δ (canopy height to boundary-layer depth) increases.

Finally, we indicate some applications for the mixing-layer analogy. First, it identifies L_s, rather than h, as the key vertical length scale for canopy turbulence and thereby rationalises the behaviour of canopies ranging from sparse (such as canopies A and Q in Figure 8) to dense (such as canopies K and L). Moreover, the canopy height h (often a hazy geometrical concept) can be given a precise aerodynamic definition as the height of the $U(z)$ inflection point. The effect of the leaf area density profile is incorporated through its influence on L_s and the ratio L_s/h.

Second, the mixing-layer analogy can be used to estimate turbulence length and time scales for applied turbulent transport models. At $z = h$, the length scale L_w is $0.71L_s$ (Figure 9). For models based on localised near-field theory (Raupach, 1989), a key parameter is the Lagrangian time scale T_L. This has been hitherto estimated as $T_L \approx 0.4h/\sigma_w \approx 0.3h/u_*$. An improved estimate can be obtained from the approximation $T_L \approx L_w/\sigma_w$ by using Equations (10) and (12) with $U_c/U_h = 1.8$ and $m = 8.1$, which gives (at $z = h$)

$$T_L \approx \frac{L_w}{\sigma_w} \approx \frac{U_h}{2\pi U_c}\frac{mL_s}{\sigma_w} \approx \frac{0.71L_s}{\sigma_w} \tag{13}$$

showing how T_L responds to canopy architecture through L_s. For a "generic" canopy with $L \approx 0.5h$, this is quite consistent with the earlier estimate.

Third, the mixing-layer analogy predicts many aspects of the behaviour of canopy turbulence in disturbed canopy environments, such as canopy edges and canopies on hills (Finnigan and Brunet, 1995). The turbulence in the upper canopy in such cases will respond to changes in the location and strength of the inflection in the mean velocity profile.

Acknowledgments

We thank Dr. M. R. Irvine for help with the additional calculations for Table IV, and Mr. P. Briggs and Mr. Greg Heath for skillful layout of the figures.

References

Amiro, B. D.: 1990a, 'Comparison of Turbulence Statistics Within Three Boreal Forest Canopies,' *Boundary-Layer Meteorol.* **51**, 99–121.

Amiro, B. D.: 1990b, 'Drag Coefficients and Turbulence Spectra Within Three Boreal Forest Canopies', *Boundary-Layer Meteorol.* **52**, 227–246.

Antonia, R. A.: 1981, 'Conditional Sampling in Turbulence Measurement', *Ann. Rev. Fluid Mech.* **13**, 131–156.

Antonia, R. A., Chambers, A. J., Friehe, C. A., and Van Atta, C. W.: 1979, 'Temperature Ramps in the Atmospheric Surface Layer', *J. Atmos. Sci.* **36**, 99–108.

Baldocchi, D. D. and Meyers, T. P.: 1988a, 'Turbulence Structure in a Deciduous Forest', *Boundary-Layer Meteorol.* **43**, 345–364.

Baldocchi, D. D. and Meyers, T. P.: 1988b, 'A Spectral and Lag-correlation Analysis of Turbulence in a Deciduous Forest Canopy', *Boundary-Layer Meteorol.* **45**, 31–58.

Bell, J. H. and Mehta, R. D.: 1990, 'Development of a Two-stream Mixing Layer from Tripped and Untripped Boundary Layers', *AIAA J.* **28**, 2034–2038.

Bergström, H. and Högström, U.: 1989, 'Turbulent Exchange Above a Pine Forest II. Organized Structures', *Boundary-Layer Meteorol.* **49**, 231–263.

Betchov, R. and Criminale, W. O.: 1967, *Stability of Parallel Flows*, Academic Press, New York, 330 pp.

Bisset, D. K., Antonia, R. A., and Raupach, M. R.: 1991, 'Topology and Transport Properties of Large-scale Organized Motion in a Slightly Heated Rough Wall Boundary Layer', *Phys. Fluids A* **3**, 2220–2228.

Blackwelder, R. F. and Kaplan, R. E.: 1976, 'On the Wall Structure of the Turbulent Boundary Layer', *J. Fluid Mech.* **76**, 89–112.

Bradshaw, P.: 1967, 'Inactive Motion and Pressure Fluctuations in Turbulent Boundary Layers', *J. Fluid Mech.* **30**, 241–258.

Browand, F. K. and Troutt, T. R.: 1980, 'A Note on Spanwise Structure in the Two-dimensional Mixing Layer', *J. Fluid Mech.* **97**, 771–781.

Brown, G. L. and Roshko, A.: 1974, 'On Density Effects and Large Structure in Turbulent Mixing Layers', *J. Fluid Mech.* **64**, 775–816.

Brunet, Y. and Collineau, S.: 1994, 'Wavelet Analysis of Diurnal and Nocturnal Turbulence Above a Maize Crop', in E. Foufoula-Georgiou and P. Kumar (eds.), *Wavelets in Geophysics*, Academic Press, New York, pp. 129–150.

Brunet, Y., Finnigan, J. J., and Raupach, M. R.: 1994, 'A Wind Tunnel Study of Air Flow in Waving Wheat: Single-point Velocity Statistics', *Boundary-Layer Meteorol.* **70**, 95–132.

Cellier, P.: 1986, 'On the Validity of Flux-gradient Relationships Above Very Rough Surfaces', *Boundary-Layer Meteorol.* **36**, 417–419.

Cellier, P. and Brunet, Y.: 1992, 'Flux-gradient Relationships Above Tall Forest Canopies', *Agric. For. Meteorol.* **58**, 93–117.

Chen, C. P. and Blackwelder, R. F.: 1978, 'Large-scale Motion in a Turbulent Boundary Layer: A Study Using Temperature Contamination', *J. Fluid Mech.* **89**, 1–31.

Chen, F. and Schwerdtfeger, P.: 1989, 'Flux-gradient Relationships for Momentum and Heat Over a Rough Natural Surface', *Quart. J. Roy. Meteorol. Soc.* **115**, 335–352.

Collineau, S. and Brunet, Y.: 1993a, 'Detection of Turbulent Coherent Motions in a Forest Canopy, Part I: Wavelet Analysis', *Boundary-Layer Meteorol.* **65**, 357–379.

Collineau, S. and Brunet, Y.: 1993b, 'Detection of Turbulent Coherent Motions in a Forest Canopy, Part II: Timescales and Conditional Averages', *Boundary-Layer Meteorol.* **66**, 49–73.

Comte, P., Lesieur, M., and Lamballais, E.: 1992, 'Large- and Small-scale Stirring of Vorticity and a Passive Scalar in a 3-D Temporal Mixing Layer', *Phys. Fluids A* **4**, 2761–2778.

Coppin, P. A., Raupach, M. R., and Legg, B. J.: 1986, 'Experiments on Scalar Dispersion Within a Model Plant Canopy, Part II. An Elevated Plane Source', *Boundary-Layer Meteorol.* **35**, 167–191.

Denmead, O. T. and Bradley, E. F.: 1985, 'Flux-gradient Relationships in a Forest Canopy', in B. A. Hutchison and B. B. Hicks (eds.), *The Forest-Atmosphere Interaction*, D. Reidel Publishing Co. Dordrecht, The Netherlands, pp. 421–442.

Denmead, O. T. and Bradley, E. F.: 1987, 'On scalar transport in plant canopies', *Irrig. Sci.* **8**, 131–149.

Dimotakis, P. E. and Brown, G. L.: 1976, 'The Mixing Layer at High Reynolds Number: Large-structure Dynamics and Entrainment', *J. Fluid Mech.* **78**, 535–560.

Drazin, P. G. and Reid, W. H.: 1981, *Hydrodynamic Stability*, Cambridge University Press, Cambridge, 527 pp.

Fiedler, H. E.: 1974, 'Transport of Heat across a Plane Turbulent Mixing Layer', *Adv. Geophys.* **18A**, 93–109.

Finnigan, J. J.: 1979a, 'Turbulence in Waving Wheat. I. Mean Statistics and Honami', *Boundary-Layer Meteorol.* **16**, 181–211.

Finnigan, J. J.: 1979b, 'Turbulence in Waving Wheat. II. Structure of Momentum Transfer', *Boundary-Layer Meteorol.* **16**, 213–236.

Finnigan, J. J. and Brunet, Y.: 1995, 'Turbulent Airflow in Forests on Flat and Hilly Terrain', *Proc. IUFRO Conf. on Wind and Wind-related Damage to Forests*, Edinburgh, 1993. In Wind and Trees (Eds M. P. Coutts and J. Grace), Cambridge University Press, Cambridge, pp. 3–40.

Finnigan, J. J., and Raupach, M. R.: 1987, 'Transfer Processes in Plant Canopies in Relation to Stomatal Characteristics', in E. Zeiger, G. D. Farquhar, and I. R. Cowan (eds.), *Stomatal Function*, Stanford University Press, Stanford, CA, pp. 385–429.

Fitzjarrald, D. R. and Moore, K. E.: 1990, 'Mechanisms of Nocturnal Exchange Between the Rain Forest and the Atmosphere', *J. Geophys. Res.* **95**, 16839–16850.

Fitzjarrald, D. R., Moore, K. E., Cabral, O. M. R., Scolar, J., Manzi, A. O., and De Abreu Sà, L. D.: 1990, 'Daytime Turbulent Exchange Between the Amazon Forest and the Atmosphere', *J. Geophys. Res.* **95**, 16825–16838.

Gao, W., Shaw, R. H., and Paw U, K. T.: 1989, 'Observation of Organized Structure in Turbulent Flow Within and Above a Forest Canopy', *Boundary-Layer Meteorol.* **47**, 349–377.

Gardiner, B. A.: 1994, 'Wind and Wind Forces in a Plantation Spruce Forest', *Boundary-Layer Meteorol.* **67**, 161–186.

Garratt, J. R.: 1978, 'Flux Profile Relations Above Tall Vegetation', *Quart. J. Roy. Meteorol. Soc.* **104**, 199–212.

Garratt, J. R.: 1992, *The Atmospheric Boundary Layer*, Cambridge University Press, Cambridge, 316 pp.

Grant, H. L.: 1958, 'The Large Eddies of Turbulent Motion', *J. Fluid Mech.* **4**, 149–190.

Ho, C., and Huerre, P.: 1984, 'Perturbed Free Shear Layers', *Ann. Rev. Fluid Mech.* **16**, 365–424.

Hunt, J. C. R. and Carruthers, D. J.: 1990, 'Rapid Distortion Theory and the 'Problems' of Turbulence', *J. Fluid Mech.* **212**, 497–532.

Inoue, E.: 1955, 'Studies of the Phenomena of Waving Plants ("Honami") Caused by Wind. Part I. Mechanism and Characteristics of Waving Plants Phenomena', *J. Agric. Met. Japan* **11**, 18–22.

Kaimal, J. C. and Finnigan, J. J.: 1994, *Atmospheric Boundary Layer Flows*, Oxford University Press, New York, Oxford, 289 pp.

Kaimal, J. C., Wyngaard, J. C., Izumi, Y., and Coté, O. R.: 1972, 'Spectral Characteristics of Surface-layer Turbulence', *Quart. J. Roy. Meteorol. Soc.* **98**, 563–589.

Leclerc, M. Y., Beissner, K. C., Shaw, R. H., Den Hartog, G., and Neumann, H. H.: 1990, 'The Influence of Atmospheric Stability on the Budgets of the Reynolds Stress and Turbulent Kinetic Energy Within and Above a Deciduous Forest', *J. Appl. Meteorol.* **29**, 916–933.

Lu, C. H. and Fitzjarrald, D. R.: 1994, 'Seasonal and Diurnal Variations of Coherent Structures Over a Deciduous Forest', *Boundary-Layer Meteorol.* **69**, 43–69.

Lu, S. S. and Willmarth, W. W.: 1973, 'Measurements of the Structure of the Reynolds Stress in a Turbulent Boundary Layer', *J. Fluid Mech.* **60**, 481–571.

Maitani, T. and Seo, T.: 1985, 'Estimates of Velocity-pressure and Velocity-pressure-gradient Interactions in the Surface Layer Over Plant Canopies', *Boundary-Layer Meteorol.* **33**, 51–60.
Maxey, M. R.: 1982, 'Distortion of Turbulence in Flows with Parallel Streamlines', *J. Fluid Mech.* **124**, 261–282.
Meyers, T. P. and Baldocchi, D. D.: 1991, 'The Budgets of Turbulent Kinetic Energy and Reynolds Stress Within and Above a Deciduous Forest', *Agric. For. Meteorol.* **53**, 207–222.
Michalke, A.: 1964, 'On the Inviscid Instability of the Hyperbolic-tangent Velocity Profile', *J. Fluid Mech.* **19**, 543–556.
Michalke, A.: 1965, 'On Spatially Growing Disturbances in an Inviscid Shear Layer', *J. Fluid Mech.* **23**, 521–544.
Monin, A. S. and Yaglom, A. M.: 1971, *Statistical Fluid Mechanics: Mechanics of Turbulence*, M.I.T. Press, Cambridge, 769 pp.
Moore, D. W., and Saffman, P. G.: 1975, 'The Density of Organized Vortices in a Turbulent Mixing Layer', *J. Fluid Mech.* **69**, 465–473.
Nakagawa, H. and Nezu, I.: 1977, 'Prediction of the Contributions to the Reynolds Stress from Bursting Events in Open-channel Flows', *J. Fluid Mech.* **80**, 99–128.
Paw U, K. T., Brunet, Y., Collineau, S., Shaw, R. H., Maitani, T., Qiu, J., and Hipps, L.: 1992, 'On Coherent Structures in Turbulence Above and Within Agricultural Plant Canopies', *Agric. For. Meteorol.* **61**, 55–68. (Corrigendum: *Agric. For. Meteorol.* **63**, 127.)
Perry, A. E., Henbest, S., and Chong, M. S.: 1986, 'A Theoretical and Experimental Study of Wall Turbulence', *J. Fluid Mech.* **165**, 163–199.
Pierrehumbert, R. T. and Widnall, S. E.: 1982, 'The Two- and Three-dimensional Instabilities of a Spatially Periodic Shear Layer', *J. Fluid Mech.* **112**, 467–474.
Priestley, C. H. B.: 1959, *Turbulent Transfer in the Lower Atmosphere*, University of Chicago Press, Chicago, 130 pp.
Qiu, J., Paw U, K. T., and Shaw, R. H.: 1995, 'Pseudo-wavelet Analysis of Turbulence Patterns in Three Vegetation Layers', *Boundary-Layer Meteorol.* **72**, 177–204.
Raupach, M. R.: 1979, 'Anomalies in Flux-gradient Relationships Over Forest', *Boundary-Layer Meteorol.* **16**, 467–486.
Raupach, M. R.: 1981, 'Conditional Statistics of Reynolds Stress in Rough-wall and Smooth-wall Turbulent Boundary Layers', *J. Fluid Mech.* **108**, 363–382.
Raupach, M. R.: 1988, 'Canopy Transport Processes', in W. L. Steffen and O. T. Denmead (eds.), *Flow and Transport in the Natural Environment: Advances and Applications*, Springer, Berlin, pp. 95–127.
Raupach, M. R.: 1989, 'A Practical Lagrangian Method for Relating Scalar Concentrations to Source Distributions in Vegetation Canopies', *Quart. J. Roy. Meteorol. Soc.* **115**, 609–632.
Raupach, M. R., Antonia, R. A., and Rajagopalan, S.: 1991, 'Rough-wall Turbulent Boundary Layers', *Appl. Mechs. Revs.* **44**, 1–25.
Raupach, M. R., Coppin, P. A., and Legg, B. J.: 1986, 'Experiments on Scalar Dispersion Within a Plant Canopy, Part I: The Turbulence Structure', *Boundary-Layer Meteorol.* **35**, 21–52.
Raupach, M. R., Finnigan, J. J., and Brunet, Y.: 1989, 'Coherent Eddies in Vegetation Canopies', *Proc. Fourth Australasian Conf. on Heat and Mass Transfer*, Christchurch, New Zealand, 9–12 May 1989.
Raupach, M. R. and Thom, A. S.: 1981, 'Turbulence in and Above Plant Canopies', *Ann. Rev. Fluid Mech.* **13**, 97–129.
Rogers, M. M. and Moser, R. D.: 1994, 'Direct Simulation of a Self-similar Turbulent Mixing Layer', *Phys. Fluids A* **6**, 903–922.
Savill, A. M.: 1987, 'Recent Developments in Rapid-distortion Theory', *Ann. Rev. Fluid Mech.* **19**, 531–575.
Seginer, I., Mulhearn, P. J., Bradley, E. F., and Finnigan, J. J.: 1976, 'Turbulent Flow in a Model Plant Canopy', *Boundary-Layer Meteorol.* **10**, 423–453.
Shaw, R. H., Brunet, Y., Finnigan, J. J., and Raupach, M. R.: 1995, 'A Wind Tunnel Study of Air Flow in Waving Wheat: Two-point Velocity Statistics', *Boundary-Layer Meteorol.* **76**, 349–376.

Shaw, R. H., Den Hartog, G., and Neumann, H. H.: 1988, 'Influence of Foliar Density and Thermal Stability on Profiles of Reynolds Stress and Turbulent Intensity in a Deciduous Forest', *Boundary-Layer Meteorol.* **45**, 391–409.

Shaw, R. H., Paw U, K. T., and Gao, W.: 1989, 'Detection of Temperature Ramps and Flow Structures at a Deciduous Forest Site', *Agric. For. Meteorol.* **47**, 123–138.

Shaw, R. H., Silversides, R. H., and Thurtell, G. W.: 1974, 'Some Observations of Turbulence and Turbulent Transport Within and Above Plant Canopies', *Boundary-Layer Meteorol.* **5**, 429–449.

Shaw, R. H., Tavangar, J., and Ward, D. P.: 1983, 'Structure of the Reynolds Stress in a Canopy Layer', *J. Climate Appl. Meteorol.* **22**, 1922–1931.

Shuttleworth, W. J.: 1989, 'Micrometeorology of Temperate and Tropical Forest', *Phil. Trans. Roy. Soc. Lond. B* **324**, 299–334.

Taylor, R. J.: 1958, 'Thermal Structures in the Lowest Layers of the Atmosphere', *Aust. J. Phys.* **11**, 168–176.

Townsend, A. A.: 1970, 'Entrainment and the Structure of Turbulent Flow', *J. Fluid Mech.* **41**, 13–46.

Townsend, A. A.: 1976, *The Structure of Turbulent Shear Flow*, Cambridge University Press, Cambridge, 429 pp.

Wallace, J. M., Eckelmann, H., and Brodkey, R. S.: 1972, 'The Wall Region in Turbulent Flow', *J. Fluid Mech.* **54**, 39–48.

Wilczak, J. M.: 1984, 'Large-scale Eddies in the Unstably Stratified Atmospheric Surface Layer. Part I: Velocity and Temperature Structure', *J. Atmos. Sci.* **41**, 3537–3550.

Wilson, J.D ., Ward, D. P., Thurtell, G. W., and Kidd, G. E.: 1982, 'Statistics of Atmospheric Turbulence Within and Above a Corn Canopy', *Boundary-Layer Meteorol.* **24**, 495–519.

Wilson, N. R., and Shaw, R. H.: 1977, 'A Higher-order Closure Model For Canopy Flow', *J. Appl. Meteorol.* **16**, 1198–1205.

Winant, C. D. and Browand, F. K.: 1974, 'Vortex Pairing: the Mechanism of Turbulent Mixing Layer Growth at Moderate Reynolds Numbers', *J. Fluid Mech.* **63**, 237–255.

Wygnanski, I. and Fiedler, H. E.: 1970, 'The Two-dimensional Mixing Region', *J. Fluid Mech.* **41**, 327–361.

Wyngaard, J. C.: 1988, 'Convective Processes in the Lower Atmosphere', in W. L. Steffen and O. T. Denmead (eds.), *Flow and Transport in the Natural Environment: Advances and Applications*, Springer, Berlin, pp. 240–260.

Zhang, C., Shaw, R. H., and Paw U, K. T.: 1992, 'Spatial Characteristics of Turbulent Coherent Structures Within and Above an Orchard Canopy', in S. E. Schwartz and W. G. N. Slinn (eds.), *Precipitation Scavenging and Atmosphere-Surface Exchange*, Hemisphere Publishing Co. Washington, pp. 741–751.